

~~SECRET~~

MRC-80-373

MRC-R-579

Copy No. 1

POSSIBLE ORIGINS OF EVENT 747 OPTICAL DATA (U)

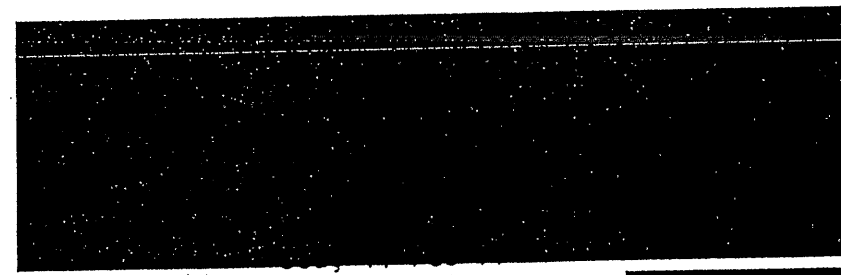
D.S. Sappenfield
D.H. Sowle
T.H. McCartor

DEPARTMENT OF ENERGY DECLASSIFICATION REVIEW	
1st REVIEW-DATE: <u>7 February 2001</u>	DETERMINATION (CIRCLE NUMBER(S)) <input checked="" type="checkbox"/> 1. CLASSIFICATION RETAINED <input type="checkbox"/> 2. CLASSIFICATION CHANGED TO: <input type="checkbox"/> 3. CONTAINS NO DOE CLASSIFIED INFO <input type="checkbox"/> 4. COORDINATE WITH: <input type="checkbox"/> 5. CLASSIFICATION CANCELED <input type="checkbox"/> 6. CLASSIFIED INFO BRACKETED <input type="checkbox"/> 7. OTHER (SPECIFY):
AUTHORITY: <u>DD</u>	
NAME: <u>Brett Palmer 58-133 (C-55)</u>	
2nd REVIEW-DATE: <u>5/7/01</u>	
AUTHORITY: <u>DD</u>	
NAME: <u>Alvino</u>	

August 1980

Prepared under Contract No. F08606-80-C-0003

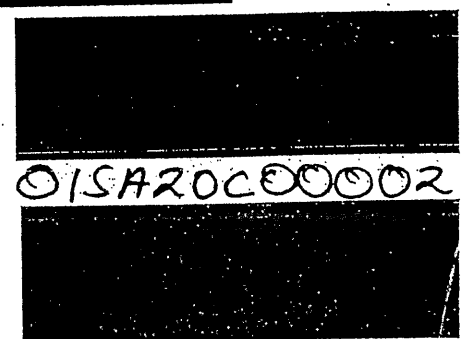
Prepared for: Air Force Technical Applications Center
Department of the Air Force
Patrick AFB, Florida 32925



AF b(2)

RESTRICTED DATA

This material contains Restricted Data as defined in the Atomic Energy Act of 1954. Unauthorized disclosure subject to administrative and criminal sanctions.



~~SECRET~~

~~SECRET~~

SECURITY CLASSIFICATION OF THIS PAGE (When Data Entered)

REPORT DOCUMENTATION PAGE		READ INSTRUCTIONS BEFORE COMPLETING FORM
1. REPORT NUMBER	2. GOVT ACCESSION NO.	3. RECIPIENT'S CATALOG NUMBER
4. TITLE (and Subtitle) POSSIBLE ORIGINS OF EVENT 747 OPTICAL DATA (U)		5. TYPE OF REPORT & PERIOD COVERED Topical Report 1 Nov 1979 - 31 July 1980
		6. PERFORMING ORG. REPORT NUMBER MRC-R-579
7. AUTHOR(s) Dale S. Sappenfield David H. Sowle Trella H. McCartor		8. CONTRACT OR GRANT NUMBER(s) F08606-80-C-0003
9. PERFORMING ORGANIZATION NAME AND ADDRESS [REDACTED] AF b(2)		10. PROGRAM ELEMENT, PROJECT, TASK AREA & WORK UNIT NUMBERS
11. CONTROLLING OFFICE NAME AND ADDRESS Air Force Technical Applications Center Department of the Air Force Patrick AFB, Florida 32925		12. REPORT DATE August 1980
		13. NUMBER OF PAGES 87
14. MONITORING AGENCY NAME & ADDRESS (if different from Controlling Office)		15. SECURITY CLASS (of this report) SRD [REDACTED]
		15a. DECLASSIFICATION/DOWNGRADING SCHEDULE
16. DISTRIBUTION STATEMENT (of this Report)		
17. DISTRIBUTION STATEMENT (of the abstract entered in Block 20, if different from Report)		
18. SUPPLEMENTARY NOTES		
19. KEY WORDS (Continue on reverse side if necessary and identify by block number) Event 747 Nuclear Test Detection		
20. ABSTRACT (Continue on reverse side if necessary and identify by block number) (S) The data recorded by VELA satellite 6911 on 22 September 1979 are analyzed in terms of both nuclear and non-nuclear sources. The objective of the analysis is to determine the relative credibilities of the two kinds of sources. While we cannot claim to have considered all possible non-nuclear sources, and we cannot absolutely rule out the non-nuclear sources that we have considered, we do not find a non-nuclear source that is a reasonable alternative to the nuclear source.		

A

~~SECRET~~

SECURITY CLASSIFICATION OF THIS PAGE(When Data Entered)

(S)

(U) Among non-nuclear sources we consider lightning, and reflections of solar radiation by small, flat plates and by irregularly shaped objects. Lightning is rejected as a source because the observed pulse widths are much longer than lightning pulse widths. Diffuse reflection from a flat plate can explain either the YC sensor data or the YV data on the second pulse, but not both simultaneously. A second reflecting plate is required to explain the first pulse.

(U) A class of irregularly shaped reflectors does exist which could produce the observed signals. These objects are highly contrived, and are subject to severe limits with respect to their location and velocity. Lacking a history of satellite observations that closely resemble observations of nuclear explosions, but which are inconsistent with one or more of the nuclear burst scaling relations, we conclude that the density of such objects is very small.

DOE b(1)

AF b(1)

SECRET

~~SECRET~~

CONTENTS

	<u>PAGE</u>
LIST OF ILLUSTRATIONS	
LIST OF TABLES	
SECTION	
1 INTRODUCTION AND SUMMARY (U)	1
2 A NUCLEAR EXPLOSION AS THE SOURCE OF THE EVENT 747 SIGNAL (S)	4
2.1 GENERAL CONSIDERATIONS	4
2.2 INFERENCES FROM THE TIMES OF MINIMUM AND SECOND MAXIMUM, "3T," AND INTEGRATED IRRADIANCE	9
2.2.1 YC DATA	9
2.2.2 YV DATA	10
2.2.3 DISCUSSION	10
2.3 INFERENCES FOR THE TIME OF FIRST MAXIMUM	12
2.4 CONCLUSIONS	24
3 NON-NUCLEAR SOURCES (U)	28
3.1 STATISTICAL DATA ON SUPERBOLT LIGHTNING PARAMETERS	29
3.2 THE FLAT PLATE	32
3.2.1 GENERAL METHOD	32
3.2.2 TRAJECTORIES TRANSVERSE TO THE OPTICAL AXIS.	34

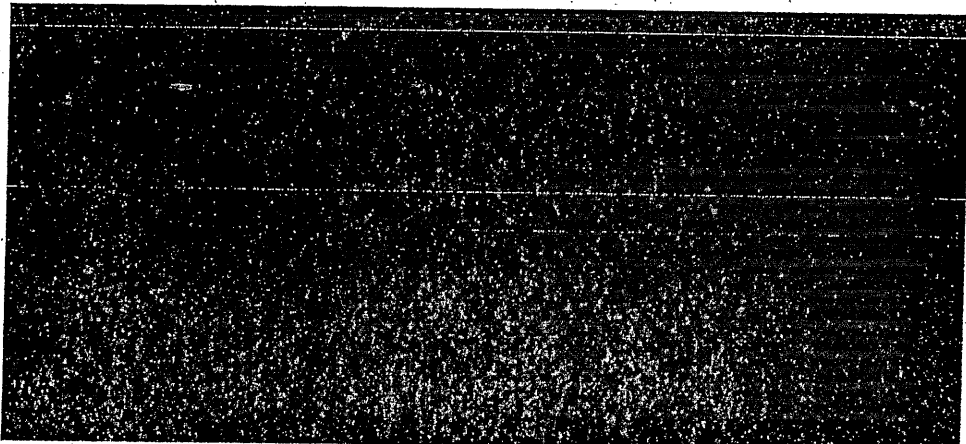
~~SECRET~~

UNCLASSIFIED

SECTION		<u>PAGE</u>
	3.2.3	TRAJECTORIES PARALLEL TO THE OPTICAL AXIS 37
	3.2.4	CONCLUSIONS 42
3.3		SINGLE OBJECT STUDY 44
	3.3.1	SUMMARY AND CONCLUSIONS 44
	3.3.2	MAJOR RESTRICTIONS ON ANY SINGLE OBJECT/ TRAJECTORY 45
	3.3.2.1	ASSUMPTIONS 45
	3.3.2.2	COORDINATES 45
	3.3.2.3	RESTRICTIONS 47
	3.3.3	EXAMPLES OF POSSIBLE OBJECTS AND ASSOCIATED TRAJECTORIES 54
	3.3.4	CREDIBILITY 67
APPENDIX A		LOCAL SOURCE ORBITAL CONSIDERATIONS FOR A SINGLE OBJECT (U) 68
REFERENCES		79

UNCLASSIFIED

LIST OF ILLUSTRATIONS

<u>FIGURE</u>		<u>PAGE</u>	
1a	(S) Event 747 data from YC sensor (U)	5	
1b	(S) Event 747 data from YV sensor (U)	6	
2	(S) Irradiance from Event 747 (U)	7	
3	(U) Theoretical power-time curve showing characteristics of veil breakthrough (U)	14	
4	(U) Theoretical power-time curve showing effects of smog absorption on the time of first maximum (U)	16	
5		-	
6		19	
7		21	
8		22	
9		23	
10		(S) Comparison of region of superbolt lightning pulses with Event 747 data (S)	25
11		(U) VELA sensor sensitivity as a function of angle (U)	30
12		(U) Computed relative irradiance produced by a flat plate moving transverse to the optical axis and approaching from the YC sensor side (U)	33
			35

DOE b(1)
AF b(1)

UNCLASSIFIED

<u>FIGURE</u>		<u>PAGE</u>
13	(U) Computed relative irradiance produced by a flat plate moving transverse to the optical axis and approaching from the YV sensor side (U)	36
14	(U) Computed relative irradiance produced by a flat plate moving transverse to the optical axis, showing the effect of constant plate rotation (U)	38
15	(U) Computed relative irradiance, 18 to 150 msec, for a flat plate moving parallel to the optical axis along a trajectory given by Equation 8 (U)	39
16	(U) Computed relative irradiance for a flat plate moving parallel to the optical axis along a trajectory given by Equations 9 and 10 (U)	40
17	(U) Computed relative irradiance, 50 μ sec to 2.5 msec, for a flat plate moving parallel to the optical axis along a trajectory given by Equation 8 (U)	43
18	(U) Coordinate system for single object study (U)	46
19	(S) Second pulse irradiance, showing different instrument responses (U)	49
20	(U) Fundamental limitation on irradiance variability (U)	51
21	(U) Multifaceted object (U)	56
22	(U) Bent rod and helix cases (U)	61
23	(U) Near field truncated sphere. Diameter \sim 1 mm (U)	64
24	(U) Truncated sphere trajectory (U)	65
25	(U) Irradiance required on detectors from truncated sphere (U)	66
A1	(U) Solution to the "first passage" perturbation equations (U)	73

UNCLASSIFIED

(S) As a consequence, our attempts to characterize non-nuclear sources for the Event 747 data either involve idealized sources, or are semi-quantitative. We believe we can show the qualitative properties of a source that are required to produce the observed signals, and we can specify some parameters quantitatively.

(S) Our principal conclusions are:

1. The optical signals recorded by both the YC and YV sensors are qualitatively, and for the most part quantitatively consistent with the signals that would be produced by a low-altitude, low-yield, nuclear explosion.

AF b(1)

2. After careful analysis of both the YC and YV sensor data in terms of a nuclear source, we conclude that the YV sensor data are the more likely to be correct. The YV sensor data imply a surface burst.

DOE b(1)
AF b(1)

3. The probability of lightning followed by a reflecting particle is low enough to disregard.
4. If one is willing to accept factor-of-2 accuracy, the YC data can be explained in terms of a pair of flat plates, behaving as "Lambert's Law radiators," that move on trajectories normal to the sensor optical axis with specific velocities and spacing. We also conclude that the YC and YV data are not simultaneously explained in these terms.

~~SECRET~~

5. A simultaneous explanation of the YC and YV data requires introduction of source surface irregularity, and some degree of specularly in the reflectivity of the surface.
6. A class of single objects and associated trajectories are conceivable which would have produced the observed data, had one been present. All members of this class are highly contrived objects with significant structural features matched to restricted trajectory; none is as simple as a sphere, rod, plate, or other common shape.
7. In the absence of a large number of multiple pulse events with nuclear-like first maxima, but obviously of non-nuclear origin, a single-particle-produced curve closely resembling a nuclear signature is most difficult to credit. Only one event satisfying the above description is known to exist prior to 747.*
8. Subjectively, we believe that the probability of a nuclear explosion, combined with a YC sensor malfunction, is much higher than the probability of any non-nuclear explanation of either or both sensor signals.

* (U) The "zoo" members are not candidates since none of them have first maxima which resemble nuclear first maxima.

~~SECRET~~

~~SECRET~~

SECTION 2

A NUCLEAR EXPLOSION AS THE SOURCE OF THE EVENT 747 SIGNAL (S)

2.1 GENERAL CONSIDERATIONS

~~(S)~~ In this section of the report we will assume that the source of the Event 747 signal is a nuclear explosion. Our purpose is to determine the characteristics of the explosion, and to see what logical difficulties, if any, follow from the assumption that the source is nuclear. We defer speculations about non-nuclear sources until Section 3.

(U) The data,¹ as recorded at the satellite, are reproduced in Figure 1. The raw data can be converted to irradiance at the sensor, using published sensor calibration curves.² Irradiance-time data are plotted in Figure 2.

~~(S)~~ The first difficulty one encounters if he assumes a nuclear source is the difference between the YC and YV sensor data during the second pulse. A distant source should deliver the same irradiance to the two sensors. While some random, or statistical differences should be expected, the difference seen in the Event 747 data is said to be well beyond what previous experience leads one to expect.³ If the source is nuclear, we have to assume that one of the two sensors behaved abnormally. This assumption complicates the analysis of the data, because we do not know a priori which sensor is giving bad data on the second pulse.

¹ J.J. McGee, letter to D.S. Sappenfield dated 7 November 1979. (S)

² R.E. Wiley and D.H. Good, "Alert 511 Optical Data Analysis (U)" AFTAC-TR-73-13, August 1973. (S)

³ J. van Workham, J.D. Marshall, private communications, November 1979. (S)

~~SECRET~~

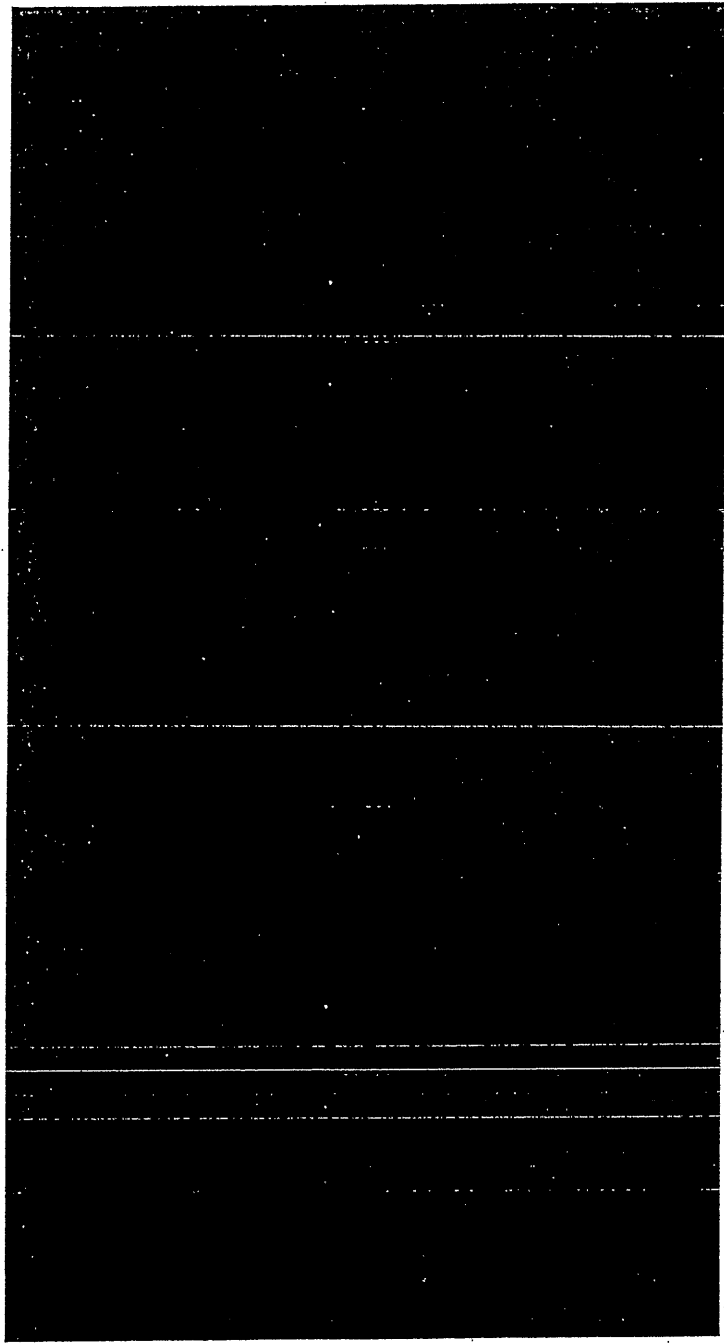


Figure 1a (U). Event 747 data from YC sensor

~~SECRET~~

DOE b(1)

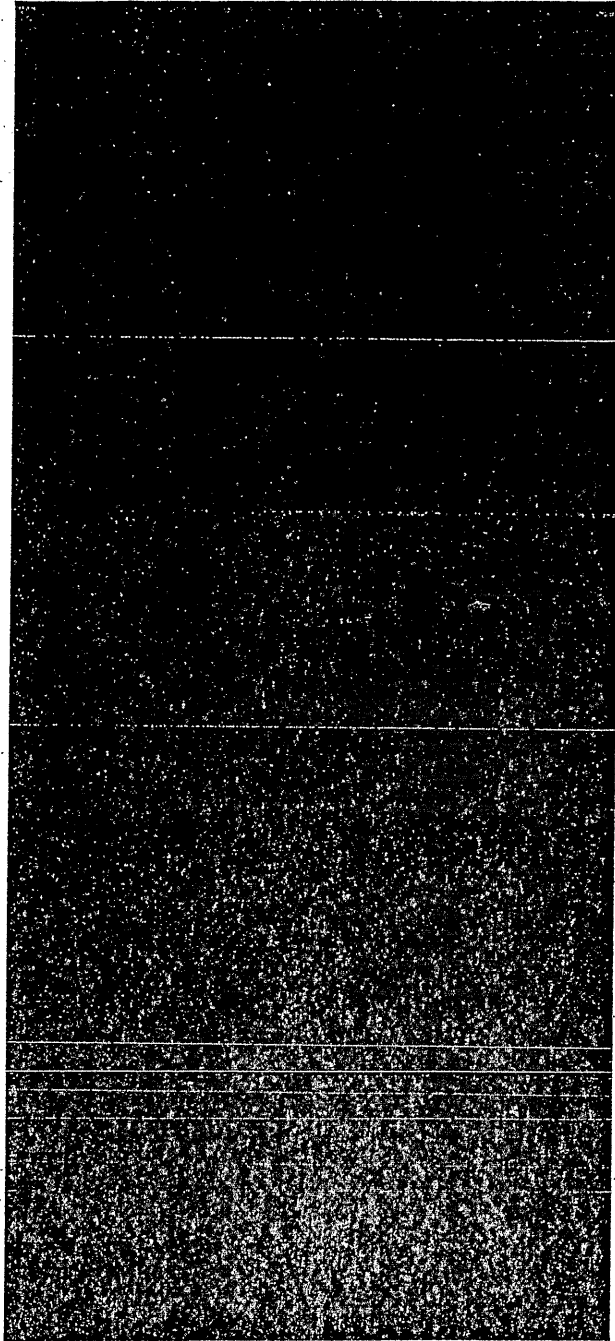


Figure 1b (U). Event 747 data from YV sensor.

~~SECRET~~

~~SECRET~~

DOE b(1)

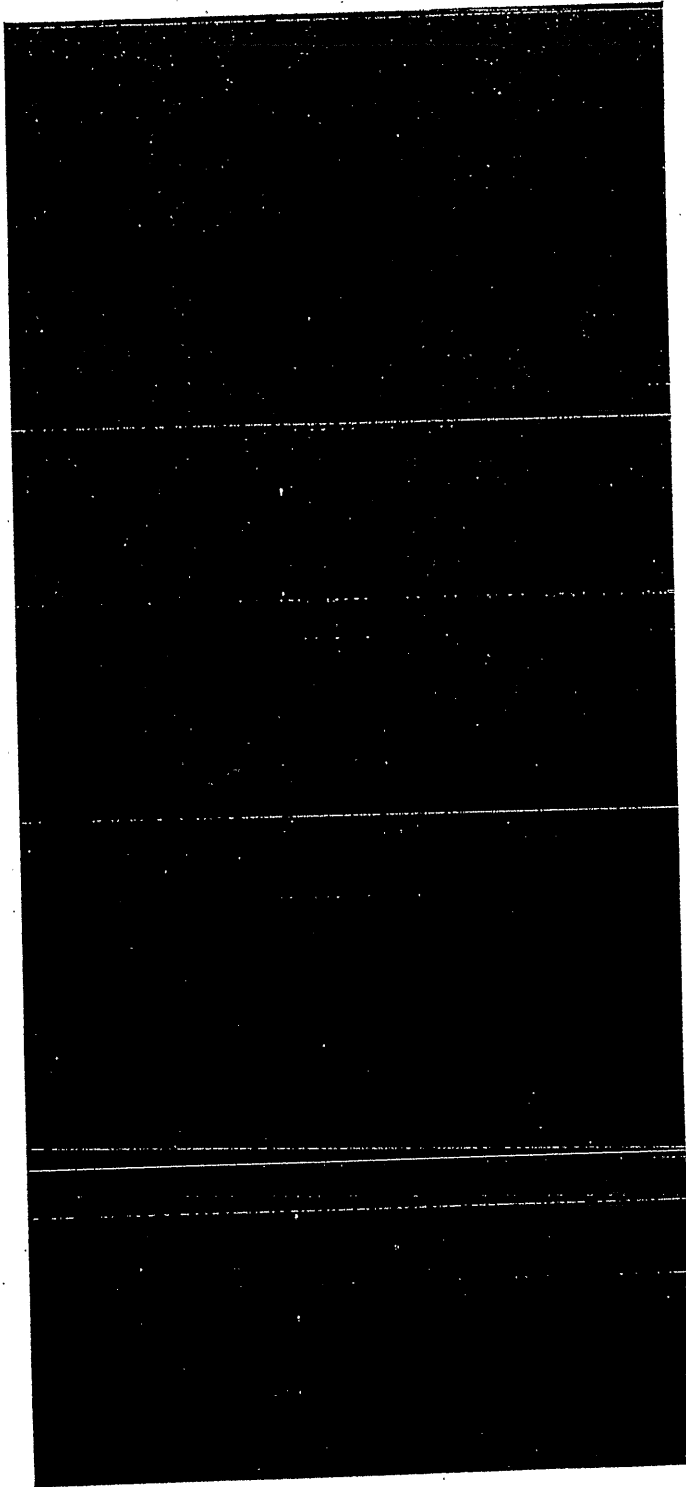


Figure 2 (U). Irradiance from Event 747

~~SECRET~~

~~SECRET~~

(S) The apparent difference between the YC and YV data during the first pulse is largely due to the difference in sensor trigger threshold, and not a cause for concern.

(S) In order to be identified as irradiance from a low-altitude, free-air, nuclear explosion, a bhangmeter curve must have two maxima. The time of the minimum, the time after minimum at which the "well" in the irradiance-time curve is a factor of 3 wide in time (known as "3T"), and the time of the second maximum, must be consistent with well-established relations⁴ between these quantities and the yield of the explosion. The energy emitted in the silicon sensor band must also be consistent with the indicated total yield of the explosion. If the source is thought to be on the surface of the earth, different scaling relations are applicable, and, if the yield is less than ~100 KT, the time of second maximum is a less well-defined function of yield.⁵

⁴ R.E. Wiley, L.W. Seiler, Jr., and J.J. Lange, "Optical Scaling Laws (U)" AFTAC-TR-80-3, January 1980. (SFRD [REDACTED])

AF b(2)

⁵ D.S. Sappenfield and T.H. McCartor, "The Surface-Burst Correction Factor for Bhangmeter Scaling Laws (U)" AFTAC-TR-79-12, March 1979. (SRD)

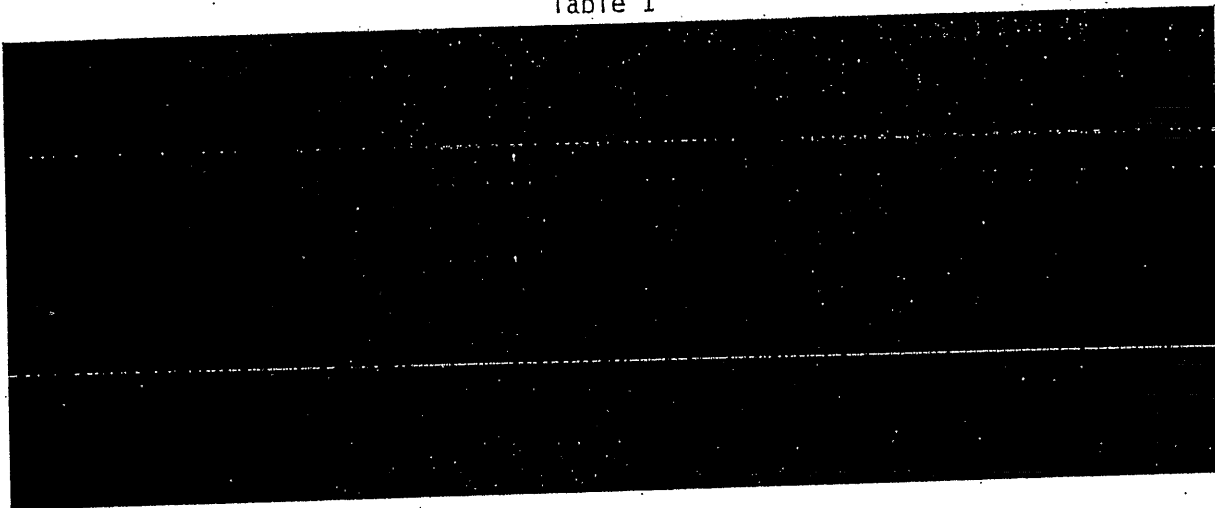
~~SECRET~~

2.2 INFERENCES FROM THE TIMES OF MINIMUM AND SECOND MAXIMUM, "3T," AND INTEGRATED IRRADIANCE

2.2.1 YC Data

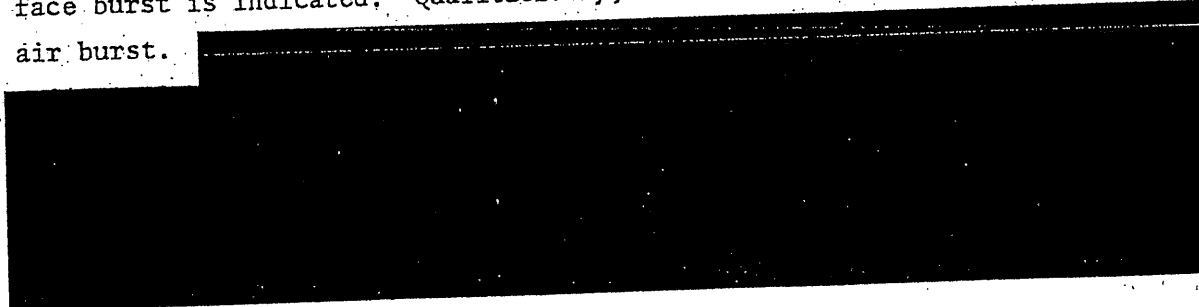
(S) Using the YC sensor data and the AFTAC scaling equations, we obtain the results shown in Table 1.

Table 1

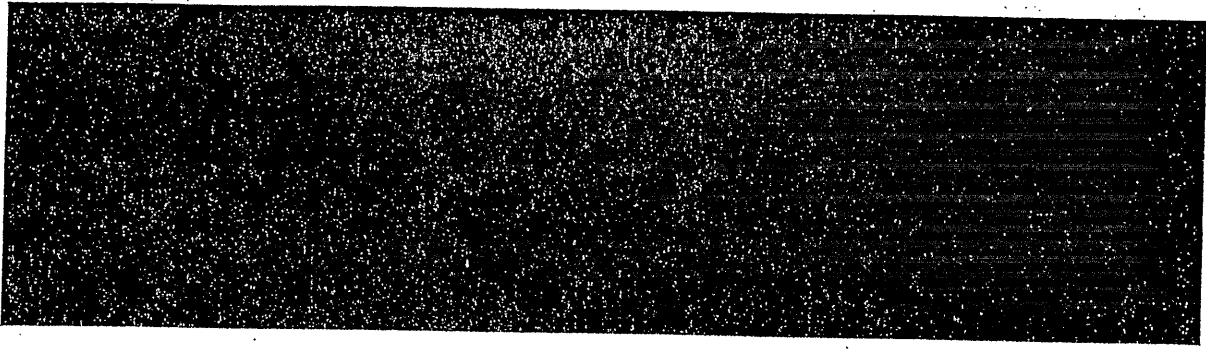


DOE b(1)
AF b(1)

(S) The relative amplitudes of the first and second maximum have been used in the past to distinguish between surface bursts and free-air bursts, at least for low yield explosions. If the amplitude of the second peak is approximately equal to or less than the amplitude of the first peak, a surface burst is indicated. Qualitatively, the YC sensor data suggest a free-air burst.

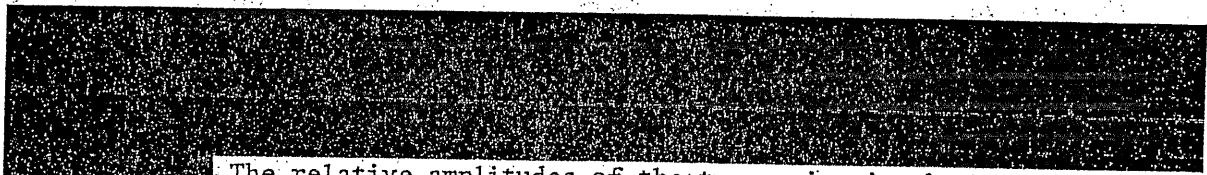


DOE b(1)
AF b(1)



DOE b(1)
AF b(1)

2.2.2 YV Data

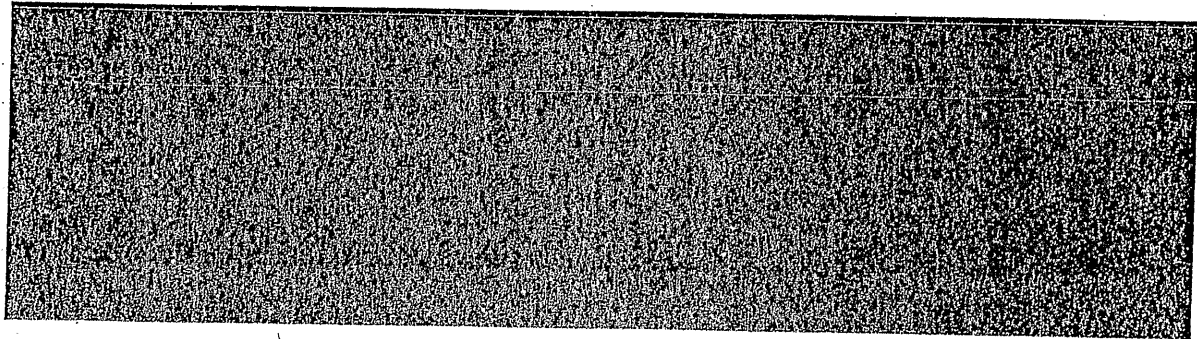


DOE b(1)
AF b(1)

The relative amplitudes of the two maxima in the YV data indicate a surface burst.

2.2.3 Discussion

(S) The yield in the silicon band is not normally used in determining the total yield of a low altitude explosion because of the uncertainty in atmospheric transmission and earth albedo, and because instrumental tail-up or tail-down can distort the measurement. Yield in the silicon band can and has been used to help distinguish between free-air and surface bursts, and it is for that reason, primarily, that we discuss it here.



DOE b(1)
AF b(1)

DOE b(1)

[REDACTED]
Observations, corrected somewhat subjectively for tail-up or tail-down, tend to be lower, presumably because of transmission losses. [REDACTED]
[REDACTED]

DOE b(1)
AF b(1)

(S) Yields in the silicon band from surface bursts are significantly smaller. Some recent data are summarized in Table 2.

Table 2
SILICON BAND YIELDS FOR RECENT SURFACE BURSTS (U)

DOE b(1)
AF b(1)

[REDACTED TABLE CONTENTS]

The smaller fractional yield observed from surface bursts presumably is caused by fireball cooling due to entrainment of surface material.

DOE b(1)

(S) [REDACTED]

The relative amplitudes of first and second maximum are consistent with this point of view. [REDACTED]

DOE b(1)
AF b(1)

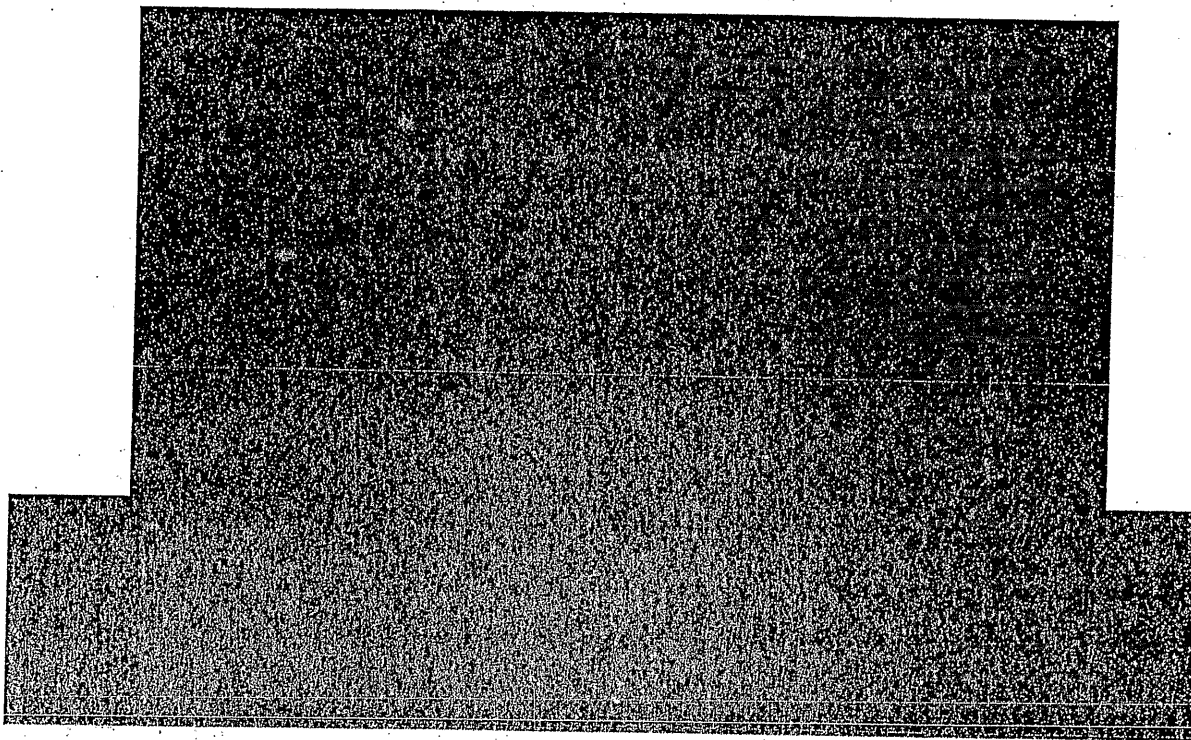
[REDACTED] The YV sensor data, on the other hand, strongly suggest a surface burst.

6 D.S. Sappenfield and T.H. McCartor, "Yield and Height of Burst Determination for High Altitude Nuclear Explosions (U)" AFTAC-TR-79-71, August 1979. (SRD)

2.3 INFERENCES FOR THE TIME OF FIRST MAXIMUM


(S) The time of first maximum, measured from the time of the YC sensor trigger, is later than usually observed for low yield events. Table 3 lists times of first maximum that have been recorded during recent years.

TABLE 3
TIMES OF FIRST MAXIMUM (U)




DOE b(1)
AF b(1)

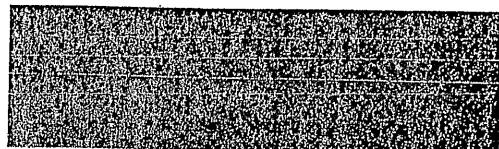
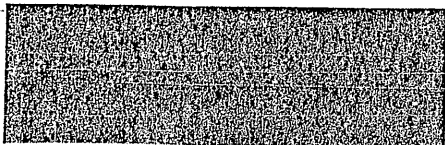
AF b(1)

7 D.S. Sappenfield, "Emplacement Effects on Optical Signals (U)", AFTAC-TR-78-14, February 1978. (S-)

AF b(2)

8 D.S. Sappenfield and T.H. McCartor, "Optical Data Evaluation Technology - Second Annual Report (U)", AFTAC-TR-79-13, March 1979. (S-)

AF b(2)



~~(S)~~ Before we regard the late first maximum in the Event 747 data as evidence for a surface burst, we should consider the ways in which the first maximum from a free-air burst can be delayed. Experimental evidence of such delays is not available for low yield explosions, as indicated by Table 3.

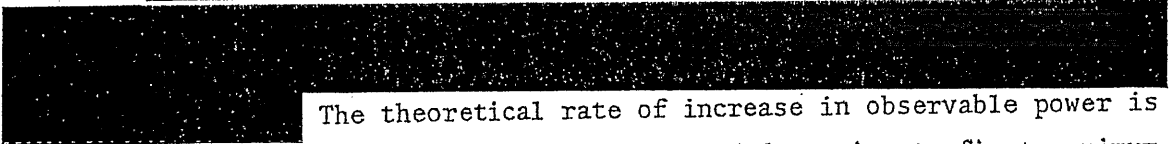


AF b(1)

~~(S)~~



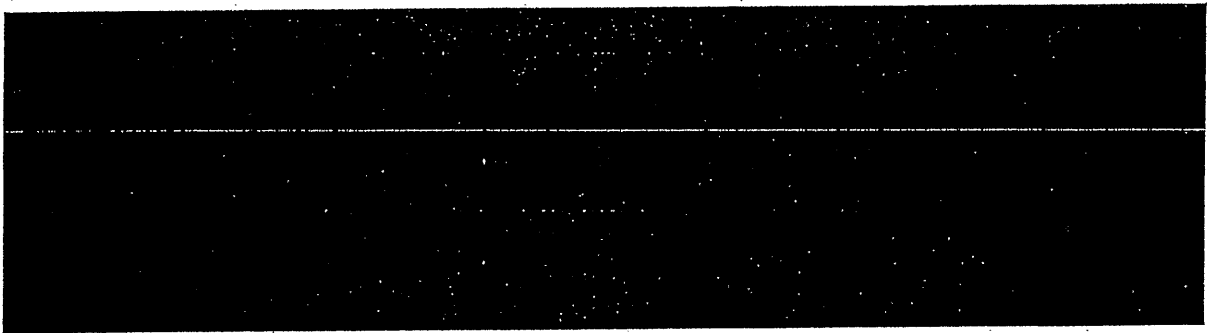
AF b(1)



The theoretical rate of increase in observable power is much faster than the rate at which the Event 747 data rise to first maximum.

DOE b(3)

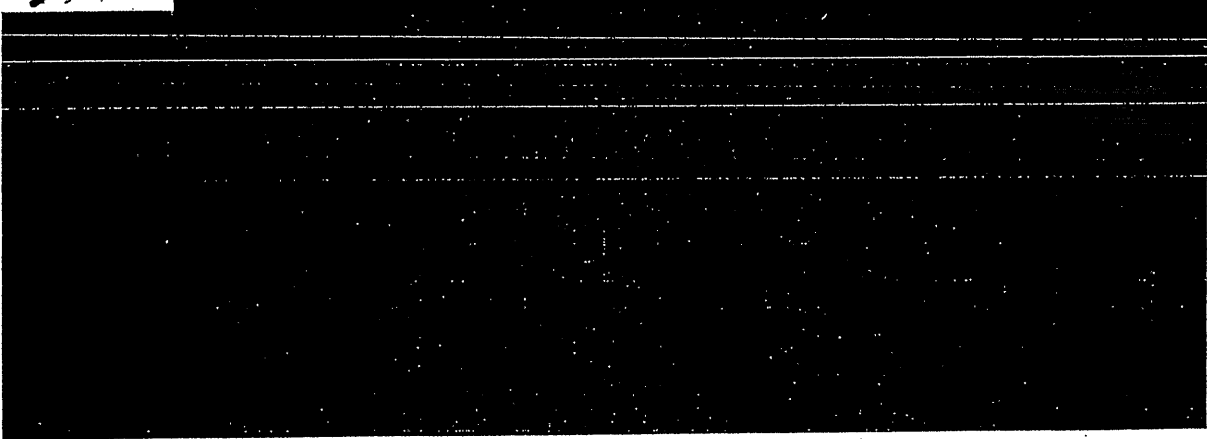
AF b(1)



~~(S)~~



AF b(1)



UNCLASSIFIED

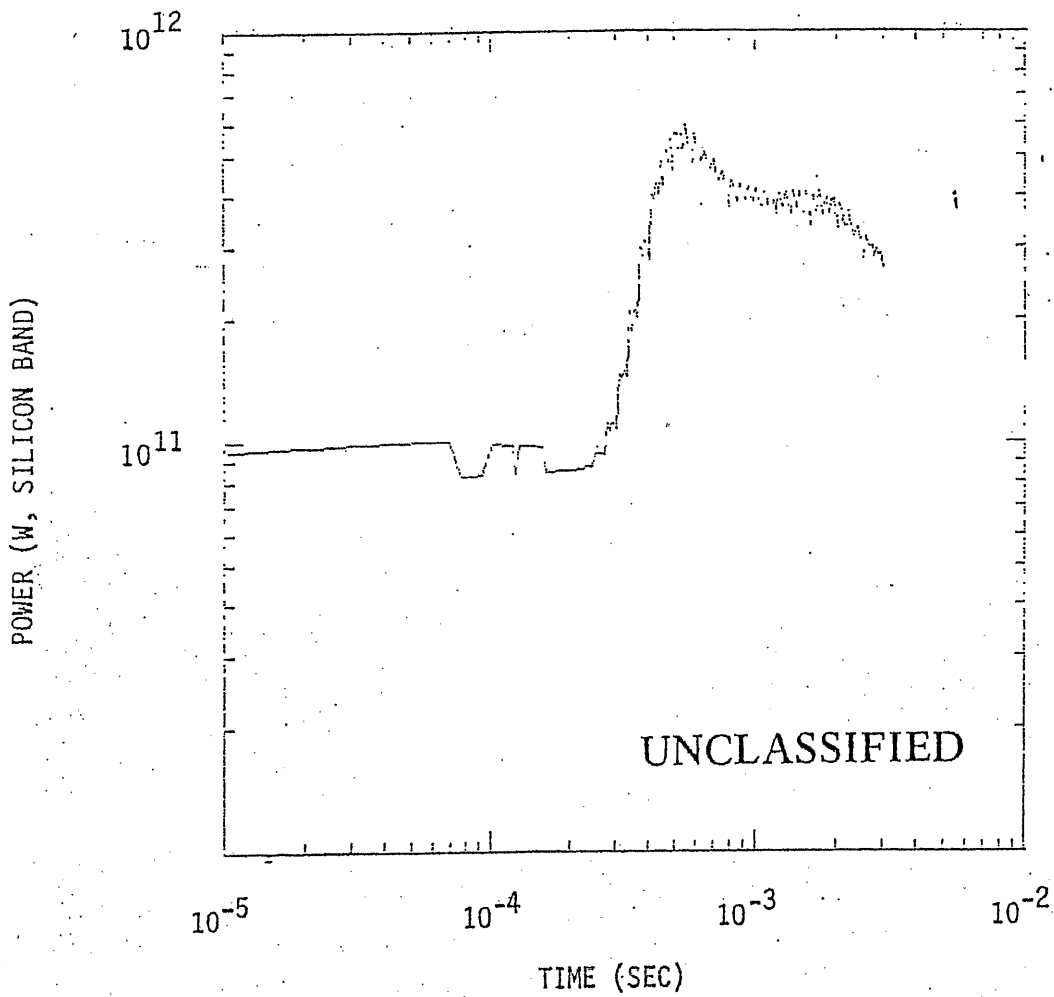
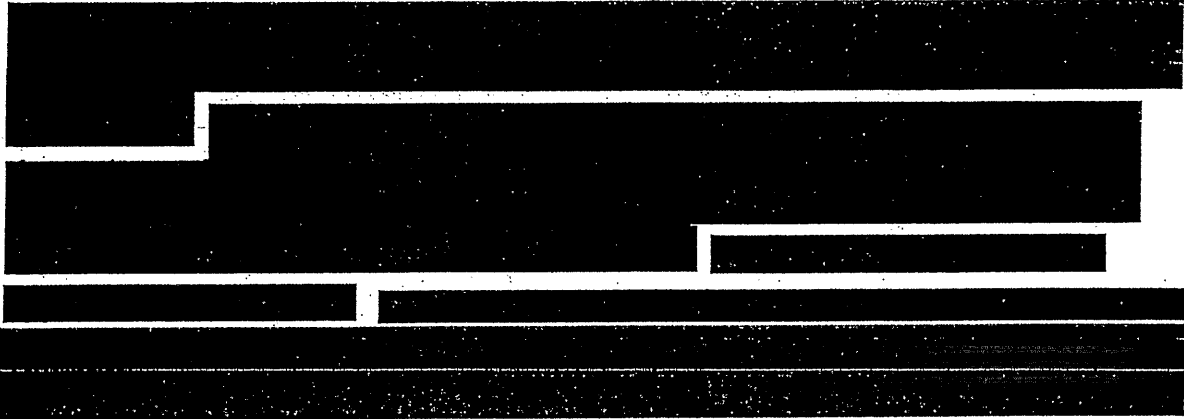


Figure 3 (U). Theoretical power-time curve showing characteristics of veil breakthrough

UNCLASSIFIED



DOE b(1)

DOE b(3)
AF b(1)

AF b(1)

DOE b(3)

(U) A very large effective weapon mass can theoretically cause the first maximum to be delayed if two conditions are satisfied. First, the mass must be sufficiently large that most of the energy of the explosion remains in the weapon material, as opposed to being radiated into the surrounding air in the form of x-rays. This condition implies a mass such that the external temperature of the weapon material is no greater than ~ 100 eV, and a sufficiently uniform distribution of mass such that there are no "hot spots," or "windows" through which radiation can flow from the probably hotter interior of the weapon. The second requirement is that the subsequent expansion of the weapon material into the air be reasonably uniform and stable.

(U) If these conditions are met, the initial expansion will resemble a momentum-conserving snowplow. Most of the weapon material internal energy will be converted rapidly into kinetic energy. The kinetic energy of the expanding debris will be converted back to internal energy as the debris is

⁹

D.S. Sappenfield and W.A. Schlueter, "Early-Time Optical Studies III (U)" Mission Research Corporation, MRC-R-178, May 1975. (SRD)

UNCLASSIFIED

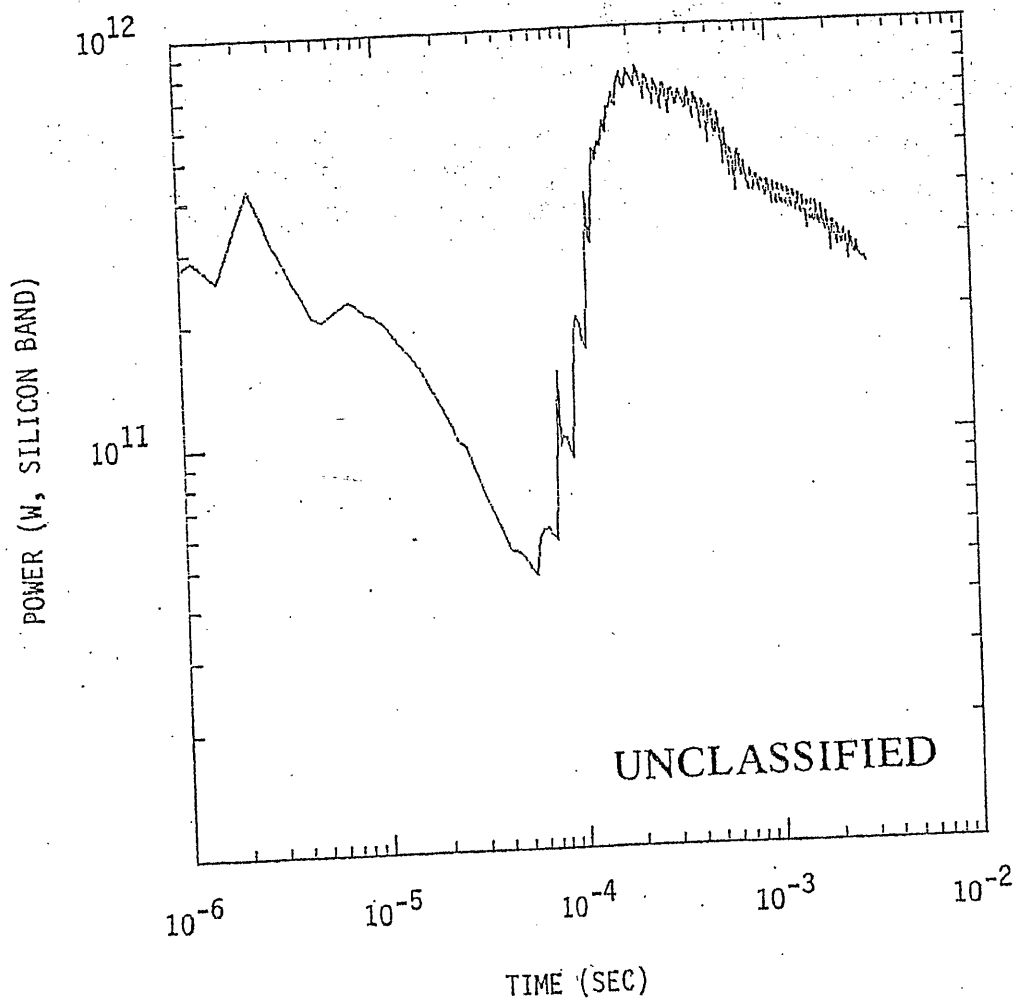


Figure 4 (U). Theoretical power-time curve showing effects of smog absorption on the time of first maximum

UNCLASSIFIED

~~SECRET~~

decelerated by the surrounding air. The maximum internal energy per unit mass will exist in the debris-air mixture when the mass of air swept up is equal to the mass of debris. The first maximum in the power should occur at about the time of the peak internal energy per unit mass, or perhaps slightly later, because of the effect of radius on the power.

DOE b(3)

For a momentum-conserving expansion,

$$\frac{dr}{dt} = M_0 v_0 / M = M_0 v_0 / (M_0 + 4\pi\rho r^3/3), \quad (1)$$

in which r is the front radius, t is time, ρ is ambient air density, 0.00129 g/cm^3 , and M_0 and v_0 are the initial debris mass and velocity. The solution can be written in the form

$$r (M_0 + 0.25[4\pi\rho r^3/3]) - M_0 v_0 t = 0 \quad (2)$$

The condition,

$$4\pi\rho r^3/3 = M_0, \quad (3)$$

together with the condition that

$$v_0 = (2Y/M_0)^{1/2}, \quad (4)$$

in which Y is the total yield, enable us to solve for the value of M_0 such that a mass, M_0 , of air is swept up by the debris in time t .

DOE b(3)
AF b(1)

If we impose the condition,

$$4\pi\rho r^3/3 = 2M_0, \quad (5)$$

~~SECRET~~

[REDACTED]

DOE b(3)
AF b(1)

[REDACTED]

DOE b(1)
DOE b(3)
AF b(1)

This energy density corresponds to a temperature of a few electron volts, and is thus consistent with our assumption.

[REDACTED]

DOE b(3)
AF b(1)

The amplitude of the observed signals has been adjusted to facilitate comparison with the calculation. The agreement between the observed and computed time of first maximum is good.

(S) At the 1980 Satellite Working Group Meeting, Whitaker and Horak¹² presented results of an Event 747 calculation. [REDACTED]

DOE b(3)

[REDACTED]
We consider the agreement between their results and our results quite satisfactory.

(U) At the same meeting, Hillendahl¹³ presented an analysis that indicates approximately an order of magnitude more mass for the Event 747 device. We do not agree with that result.

- 10 J. Zinn, J. Comp. Phys., 13, 569 (1973). (U)
- 11 D.S. Sappenfield, "Early-Time Optical Studies IV (U)" Mission Research Corporation, MRC-R-283, September 1976. (S)
- 12 R. Whitaker and H. Horak, "Calculations..... (U)" Paper presented at the Satellite Working Group Meeting, PAFB, 18-20 March 1980. (S)
- 13 R. Hillendahl, "Interpretation..... (U)" Paper presented at the Satellite Working Group Meeting, PAFB, 18-20 March 1980. (S)

DOE b(1)
AF b(1)

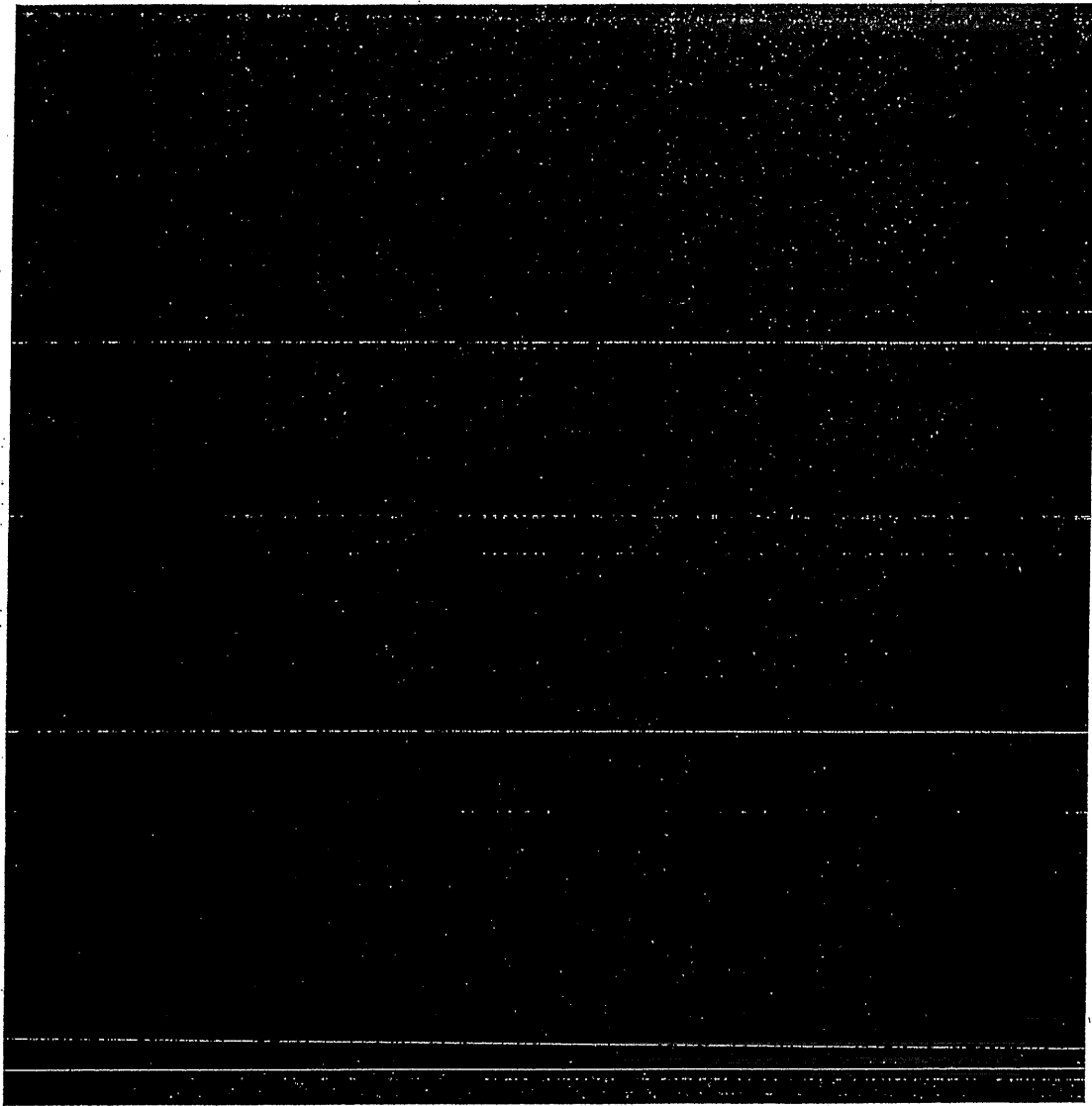


Figure 5 ~~(S)~~.



DOE b(1)
DOE b(3)

~~SECRET~~

(S) U.S. nuclear test data do not provide a very critical test of the theoretical argument relating the time of first maximum to device mass.

[REDACTED]

DOE b(1)
DOE b(3)
DOE b(1)

[REDACTED]

DOE b(1)

[REDACTED]

DOE
b(3)

[REDACTED] The observed power-time curve, computed for the silicon band from spectral power measurements¹⁵, is shown in Figure 8. Again, the agreement with the predicted time of first maximum is good, but the effect of the bomb mass in delaying the maximum is not large.

¹⁴ P.B. Wells, et al., "Nuclear Weapons Thermal Radiation Phenomena (U)" DNA 2500H-2, July 1974. (SRD)

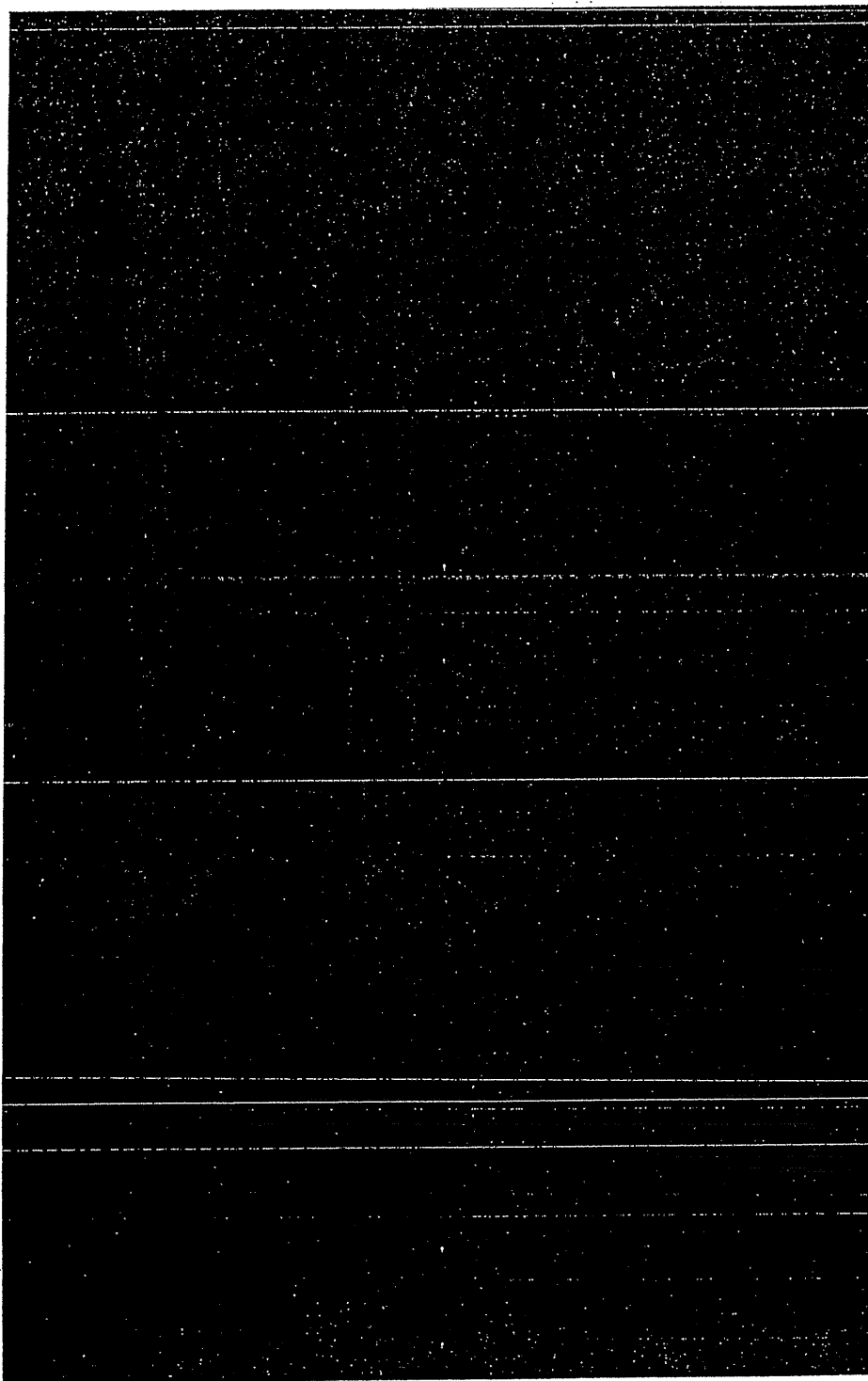
¹⁵ W.L. Derksen and F.C. DeBold, "Measured Spectral Powers for Ten Low Altitude Nuclear Bursts (U)" DASA-1663-4, January 1972. (SFRD)

~~SECRET~~

~~FORMERLY
RESTRICTED DATA~~

~~SECRET~~

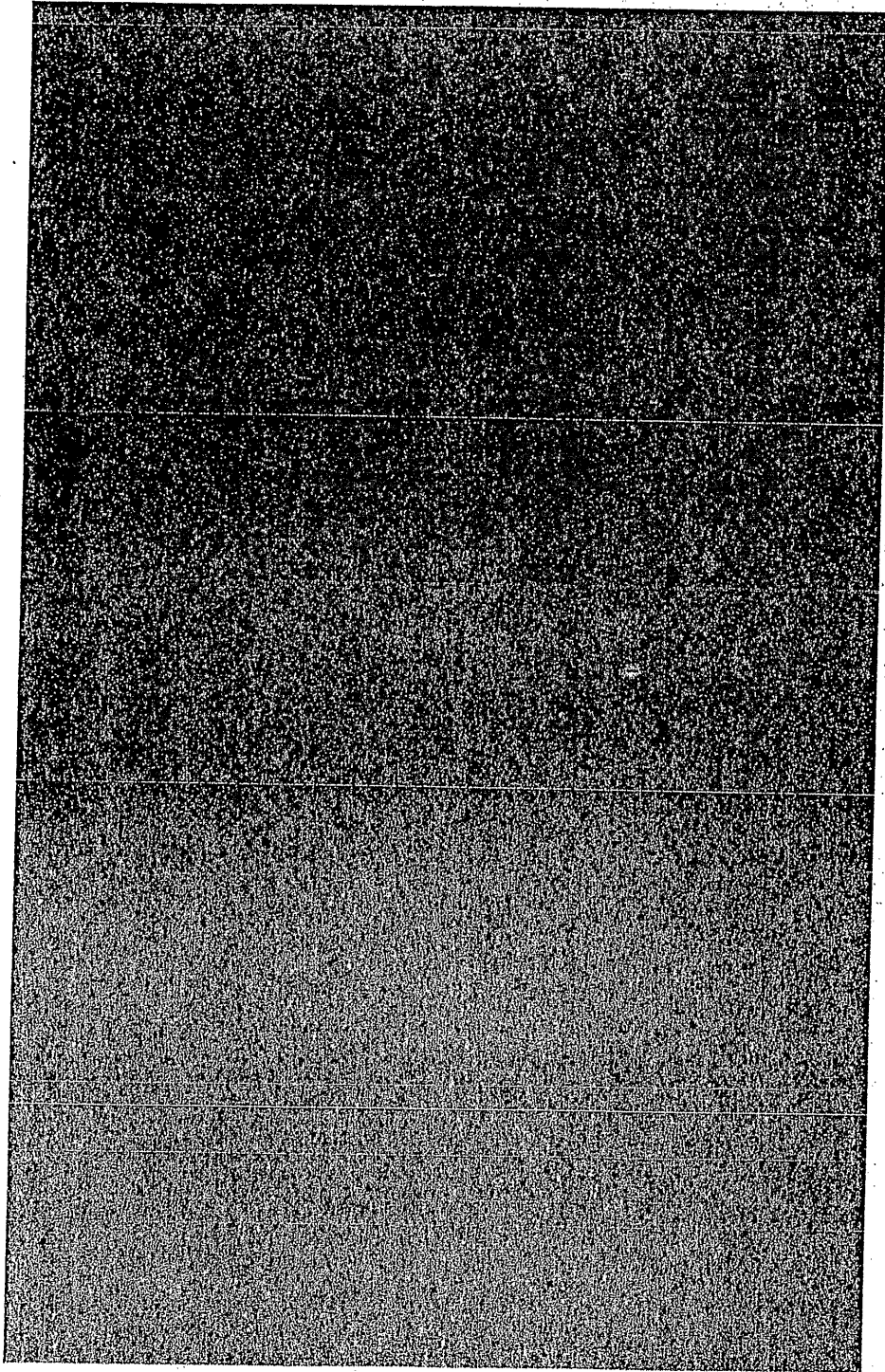
DOE b(1)



~~SECRET~~

~~SECRET~~

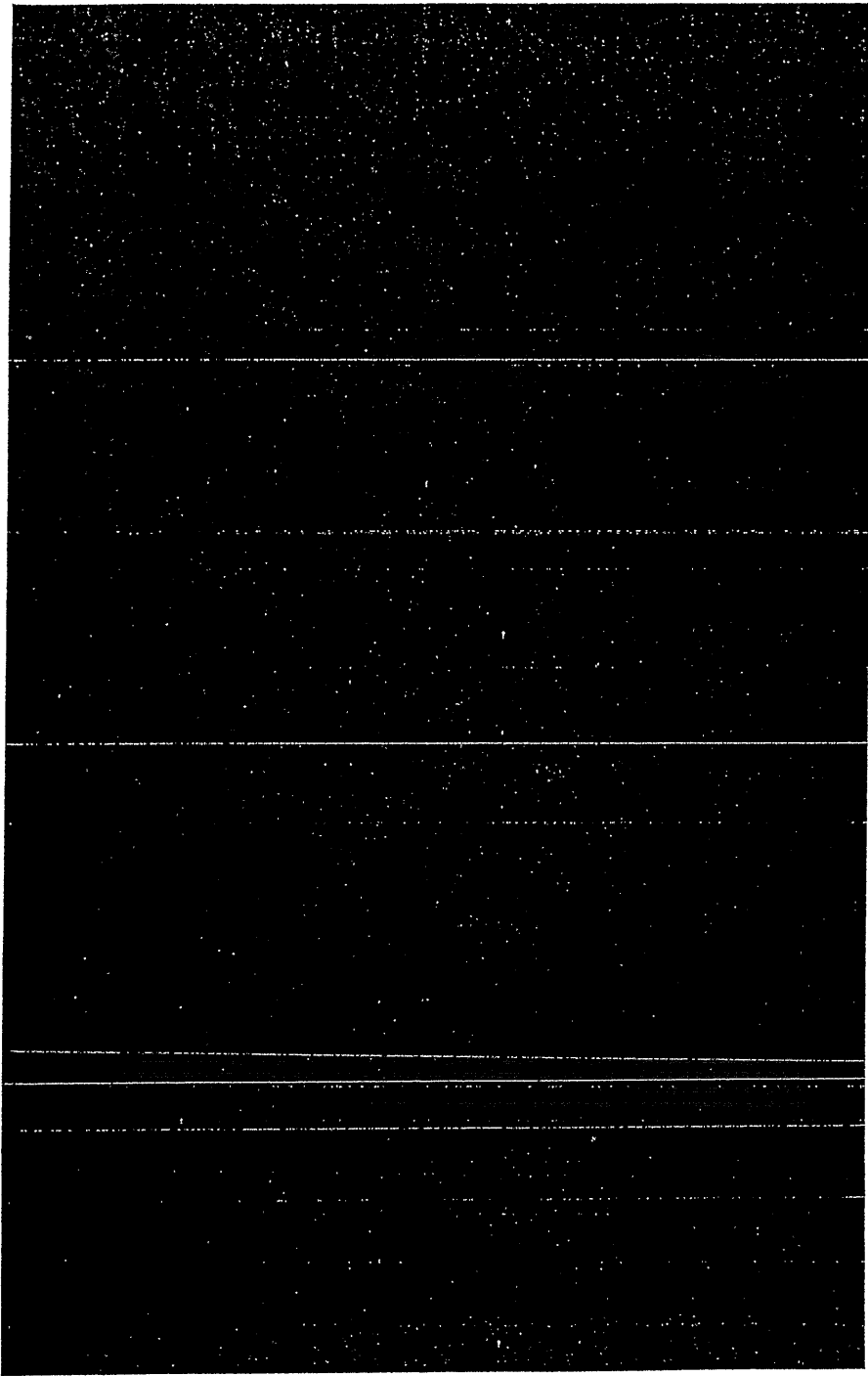
DOE b(1)



~~SECRET~~

~~SECRET~~

DOE b(1)




~~SECRET~~

~~SECRET~~

2.4

CONCLUSIONS

DOE b(3)

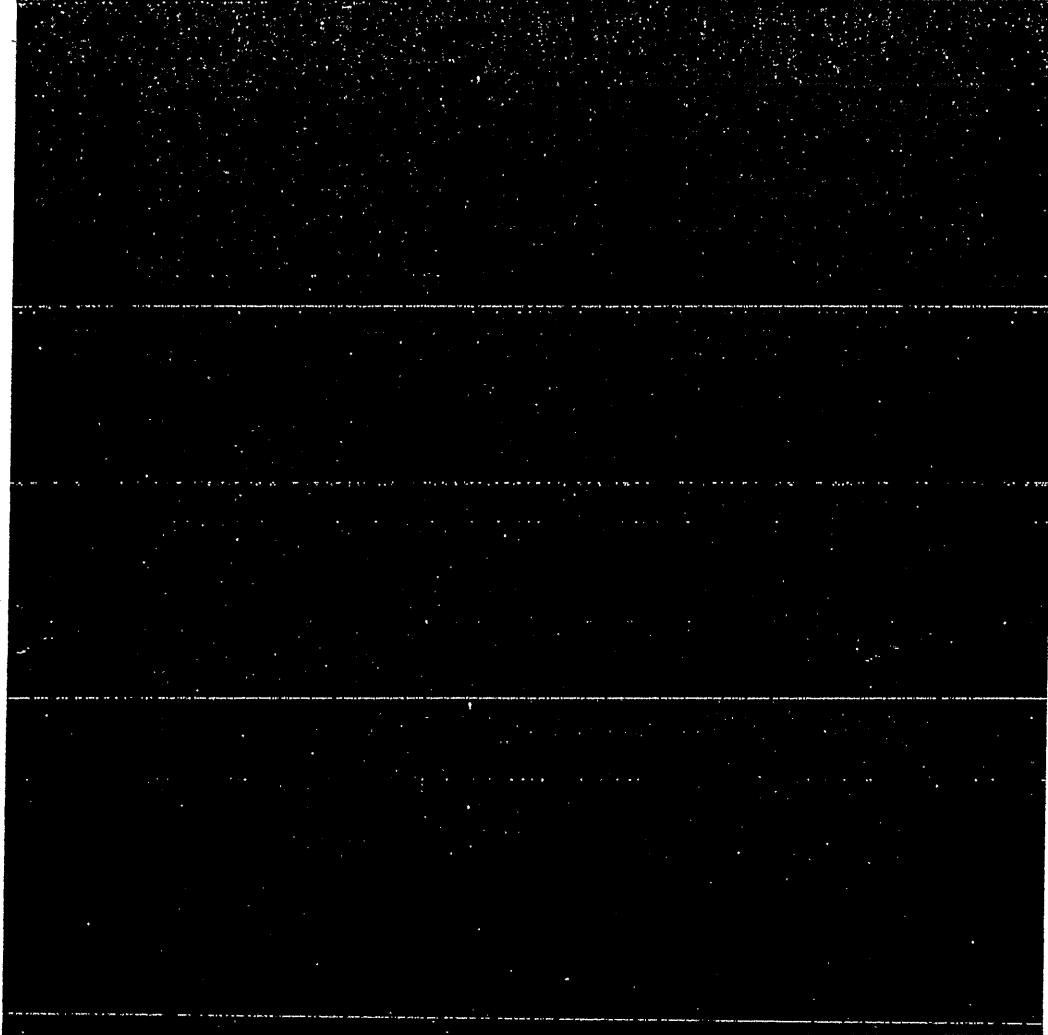


Additional doubts are raised when we compare on an absolute basis the Event 747 data with computed power-time curves. The measured irradiance can be converted to power by multiplying the irradiance by 4π times the square of the distance between the source and sensor, and by applying a correction for atmospheric transmission loss and earth or cloud albedo.

(U) In Figure 9 we show a comparison of calculation and observation, in which the observed irradiance has been multiplied by $4\pi \times (1.1 \times 10^{10})^2 \text{ cm}^2$, the approximate distance of the satellite from the earth. The difference in amplitude between the computed and "observed" curves is then a measure of the combined air transmission and albedo corrections. The results shown in Figure 9 indicate a combined correction factor of ~ 1.7 , if we believe the YC sensor data. This result is very nearly incredible, because the atmospheric transmission correction must be less than unity, and the albedo correction for a detonation above a plane mirror is only 2.0.

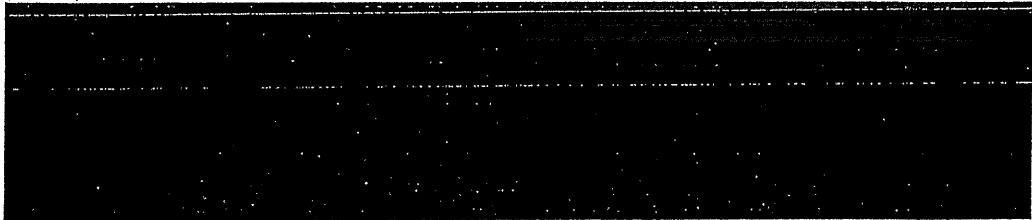
(U) It is true, of course, that we could increase the computed power by increasing the yield of the explosion. Peak power at second maximum scales approximately as the square root of the yield (because the time of second maximum also scales (approximately) as the square root of the yield, and the integral of the power-time curve is very nearly proportional to yield), so that the yield would have to be increased by about a factor of 3 in order to reduce the combined atmospheric transmission and albedo factor to 1.0. However, if yield were increased a factor of 3, the computed times of minimum and second maximum, as well as "3T," would no longer agree with the observations.

~~SECRET~~



DOE b(1)
AF b(1)

Figure 9 ~~(S)~~.



AF b(1)
DOE b(1)
DOE b(3)

(S) In summary, we find that the assumption that the YC sensor data are correct leads to an implausible (but not impossible!) picture of the source. If, on the other hand, one assumes that the YV sensor data are correct, he can deduce a self-consistent description of the source, albeit one that is somewhat incomplete owing to the sensor's failure to measure the time of minimum. It is interesting to note that everyone we know who has looked at the Event 747 data first accepted and concentrated on the YC sensor data. However, by the time of the 1980 Satellite Working Group Meeting, not only we, but Mauth,¹⁶ and Marshall,¹⁷ were tending toward the view that the YV sensor data are more trustworthy. Furthermore, these opinions were reached independently, as far as we know, and were based on different lines of reasoning.

(S-) Using the YV sensor data, we concluded that Event 747 was a surface burst. [REDACTED]

[REDACTED]

[REDACTED]

AF b(2)
DOE b(1)
AF b(1)

DOE b(1)
AF b(1)

16 G. Mauth, Informal presentation at the Satellite Working Group Meeting, PAFB, 16-18 March 1980. (S)

17 J.D. Marshall, "Statistical Analysis (U)" paper presented at the Satellite Working Group Meeting, PAFB, 16-18 March 1980. (S)

18 S. Chavin, T.H. McCartor and D.S. Sappenfield, "Yield and Depth of Burial Determination for Shallow-Buried Nuclear Bursts (U)" AFTAC-TR-78-49, July 1978. (S-)

AF b(2)

[REDACTED]

AF b(2)

minimum measured by the YC sensor. We question its validity not only because we have already decided that the YC sensor misbehaved during Event 747, but for two other reasons as well. [REDACTED]

DOE b(1)
AF b(1)

(S) Our upper limit on the yield is based on observations of the extent to which the time to second maximum can be shortened for a low yield surface burst. [REDACTED]

DOE b(1)
AF b(1)

[REDACTED] In this case, the integrated yield in the YV sensor band would be a little low, but not unreasonable in view of the generally cloudy weather thought to exist in the burst region.

DOE b(1)
AF b(1)

[REDACTED]

[REDACTED]

DOE b(1)
AF b(1)

19 L.W. Seiler, Jr., J.A. Van Workham and N.P. Philliber, "Satellite Data Summary - [REDACTED] AFTAC-TR-79-9, March 1979. (S)

AF b(2)

UNCLASSIFIED

SECTION 3 NON-NUCLEAR SOURCES

(U) In this section we consider three kinds of non-nuclear sources that, in principle, could produce the Event 747 data.

(U) Because lightning is known to be a source of false triggers, we consider the possibility that the first peak in the data is caused by a so-called "superbolt." Lightning is ruled out as the cause of the second peak because of the duration and optical energy in the second peak.

(U) Solar irradiance, reflected into the VELA sensors by objects near the satellite, is sufficiently intense by several orders of magnitude to produce sensor triggering, provided certain time tests are met. There is a continuum of possible reflectors that might be considered. We will discuss two classes of reflectors. At Dr. Leies's suggestion, we consider flat surfaces, or plates, that reflect or scatter sunlight according to Lambert's Law. We also consider irregularly-shaped, specular reflectors.

3.1 STATISTICAL DATA ON SUPERBOLT LIGHTNING PARAMETERS

(S) VELA satellites have recorded optical signals which are characteristic of lightning as well as the characteristic flash from nuclear tests. Thus a possible explanation for [REDACTED] Event 747 is a superbolt—a lightning flash at least 100 times more powerful than "typical" lightning.²⁰

AF b(1)

DOE b(1)

[REDACTED]

It is further asserted that superbolts occur in maritime atmospheres and carry positive charge to the earth; this is in contrast to the majority of lightning flashes which carry negative current to ground.²¹

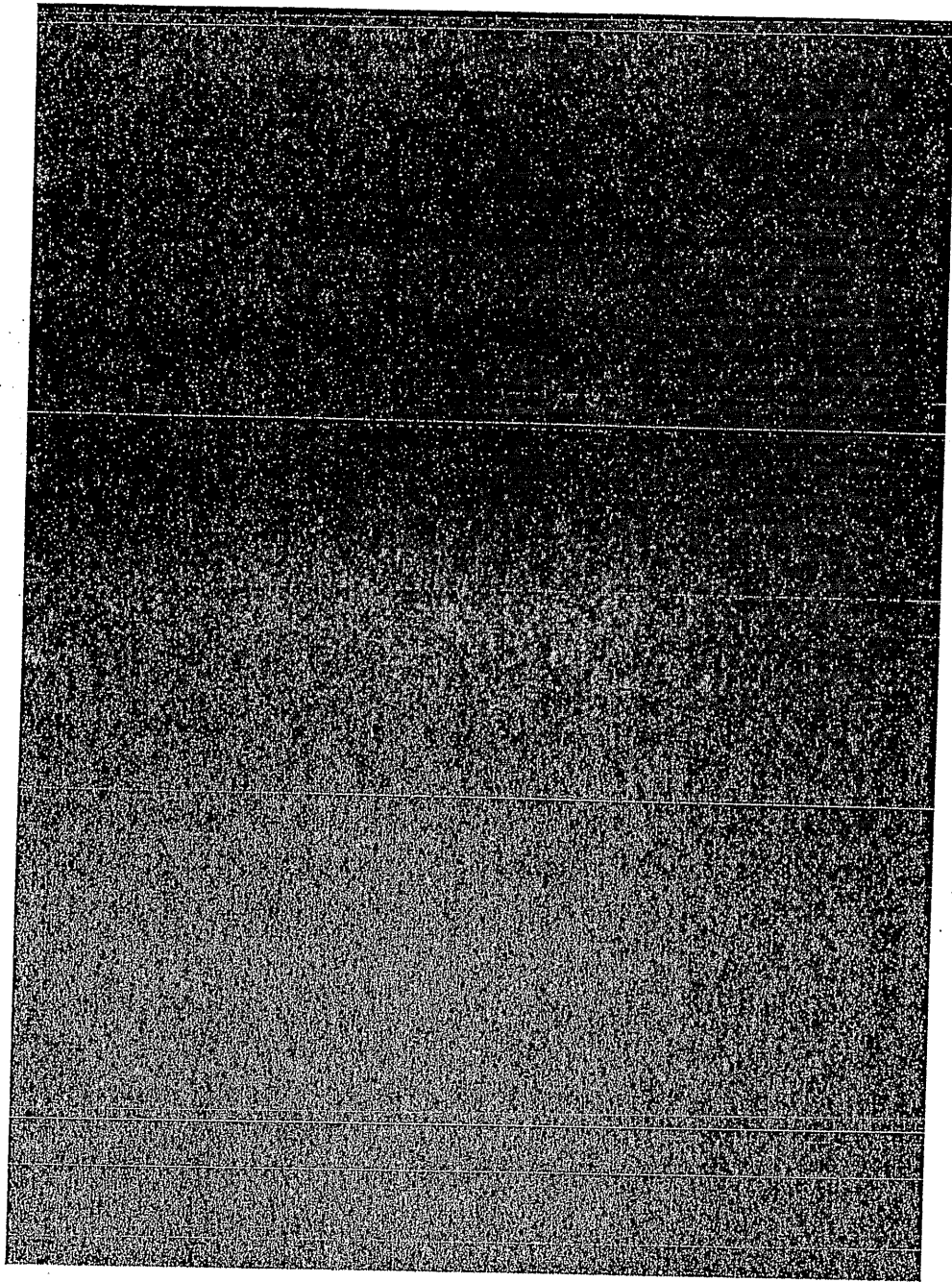
(U) Edgar²² presents data taken by the optical sensor aboard the DMSP satellite which has sensors that are a factor of 100 more sensitive than VELA sensors. He states that 7 percent of the detected lightning strokes have duration times greater than 1000 μ sec, which he asserts is consistent with Uman's²³ statistics of groundbased observations of positive strokes made by various investigators. Due to threshold sensitivity differences between DMSP and VELA, these duration time statistics are compatible to

20 Turman, B.N., "Detection of Lightning Superbolts," J. Geophys. Res., 82, 2566 (1977). (U)

21 Turman, B.N., "Lightning Detection From Space," Am. Sci., 67, 321 (1979). (U)

22 Edgar, B.C., "Global Lightning Distribution at Dawn and Dusk for August-December 1977 as Observed by the DMSP Lightning Detector," The Aerospace Corporation, SSL-78(3639-02)-1, August 1978. (U)

23 Uman, M.A., Lightning, McGraw-Hill Book Company, New York, 1979. (U)



DOE b(1)
AF b(1)

Figure 10 (S). Comparison of region of superbolt lightning pulses with Event 747 YC data. Note: [REDACTED]
[REDACTED]

AF b(1)

~~SECRET~~

within a factor of 2 to 3. Even though the total amount of superbolt data is limited, the data exhibit good statistical correlation.

(S) A comparison of the superbolt data with the Event 747 first pulse data is shown in Figure 10.

DOE b(1)
AF b(1)

Except for differences that are explainable in terms of the lower sensor sensitivity, the data from the YV sensor are similar to the YC sensor data. The peak optical power is reasonable for a superbolt; the duration time and total energy are large. Since the Event 747 data has a duration time more than 4 times longer than the upper limit quoted by Turman for VELA sensors and a total energy 2 times greater, we regard the probability that the first peak was caused by a superbolt as negligible.

~~SECRET~~

3.2 THE FLAT PLATE

3.2.1 GENERAL METHOD

(S) At the suggestion of Dr. Leies, we have looked at reflection from flat plates as a possible explanation of the observed signals. We recognize immediately that two such plates are required, one to produce each peak, and that their passages across the field of view must be synchronized to produce the proper time interval between the peaks.

(U) If we assume that the plates are perfectly flat, and are "Lambert's Law radiators," we can compute relative irradiance at the VELA sensors as a function of time as the plates move across the field of view. Specifically,

$$I \approx S(\theta) \cos(\phi)/r^2 \quad , \quad (6)$$

in which θ is the angle between the instantaneous line of sight and the normal to the plane that contains the sensors, ϕ is the angle between the line of sight and the normal to the plate, $S(\theta)$ is the dependence of sensor sensitivity on look angle,²⁴ which is plotted in Figure 11, r is the distance between the plate and the sensor, and the plate is small enough to be treated as a point source. We assume that the sensors lie in the $x=0$ plane, along the y axis. The YV sensor coordinate is $(0, -0.154, 0)$; the YC sensor coordinate is $(0, 0.154, 0)$, with distances in meters. Although an infinite number of plate trajectories are possible, we have examined only two classes of trajectory: trajectories normal to the optical axis and trajectories parallel to the optical axis. Results for trajectories at other angles can to some extent be estimated from these limiting cases.

²⁴ Marshall, J.D., private communication, December 1979. (U)

UNCLASSIFIED

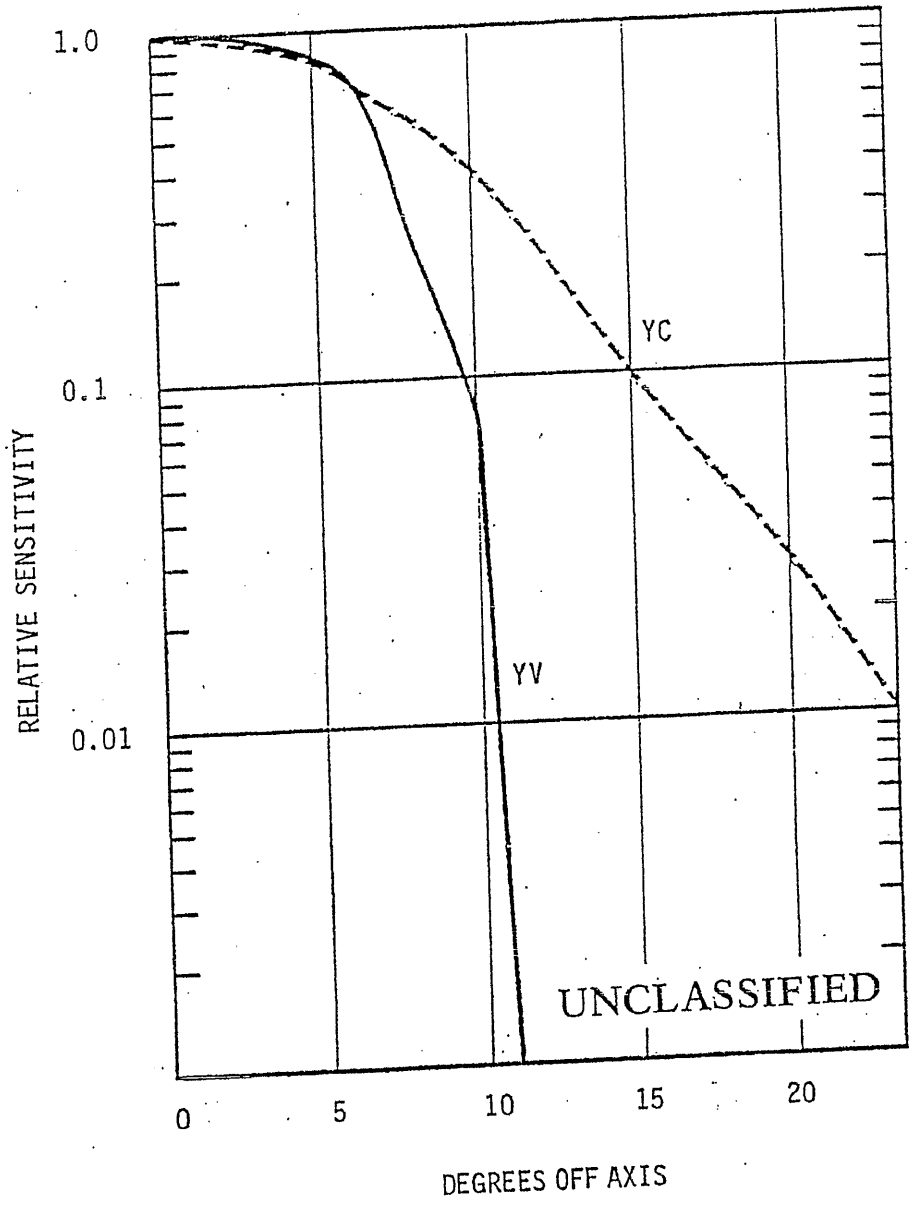


Figure 11 (U). VELA sensor sensitivity as a function of angle

UNCLASSIFIED

~~SECRET~~

3.2.2 TRAJECTORIES TRANSVERSE TO THE OPTICAL AXIS

(U) We assume that the plate moves in the y direction at a constant distance, x , from the sensors. Typical results are shown in Figures 12 and 13. In both cases the equations of the line along which the plate moves are

$$x = 10, \quad z = 0 \quad (7)$$

In other words, the plate passes directly in front of the sensors at a distance of 10 m. In Figure 12 the plate is moving in the $-y$ direction; in Figure 13 the plate moves in the $+y$ direction. The plate is parallel to the sensor plane.

(U) The peak amplitude and time scale are adjusted so that the leading edge of the first peak in the YC sensor curve is matched as well as possible. This adjustment involves an arbitrary constant by which all amplitudes are multiplied, and the definition of the velocity with which the plate is moving. For these transverse trajectories, required velocity is proportional to the distance of closest approach of the plate. For our case the closest approach is 10 m, and the required angular velocity is 4000 m/sec., or about twice escape velocity at VELA satellite altitude.

(S) These curves show the principal problem with the transverse trajectory. Except for minor perturbations produced by the separation of the YC and YV sensors, the rise and fall of irradiance is linearly symmetric around the time of peak irradiance. Neither peak in the Event 747 data shows such symmetry, and consequently, the data are not consistent with flat plates that move normal to the optical axis.

(U) A slight expansion of the late-time part of the irradiance curve can be achieved by rotating the plate relative to the sensor plane, so that

~~SECRET~~

UNCLASSIFIED

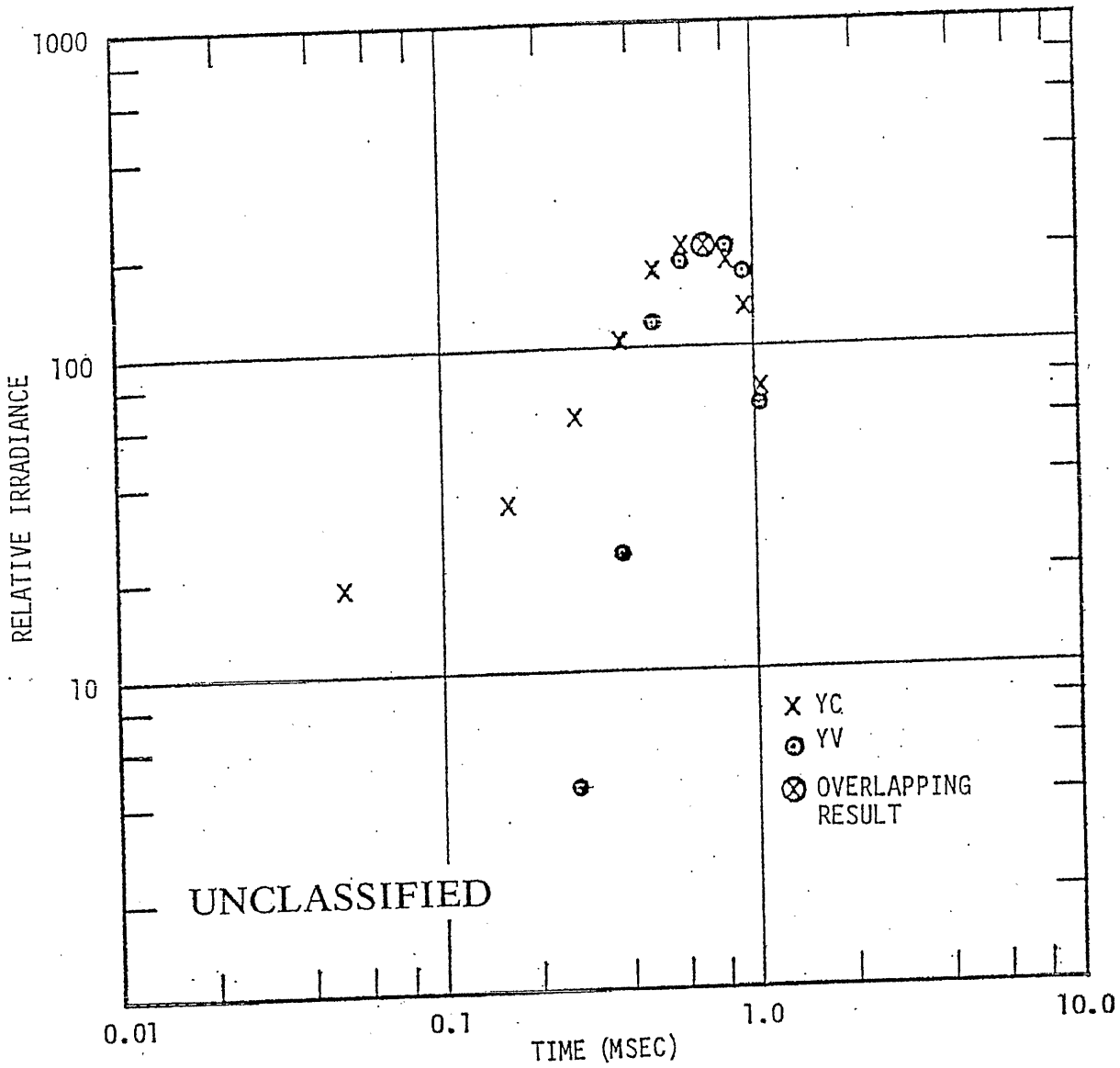


Figure 12 (U). Computed relative irradiance produced by a flat plate moving transverse to the optical axis and approaching from the YC sensor side

UNCLASSIFIED

UNCLASSIFIED

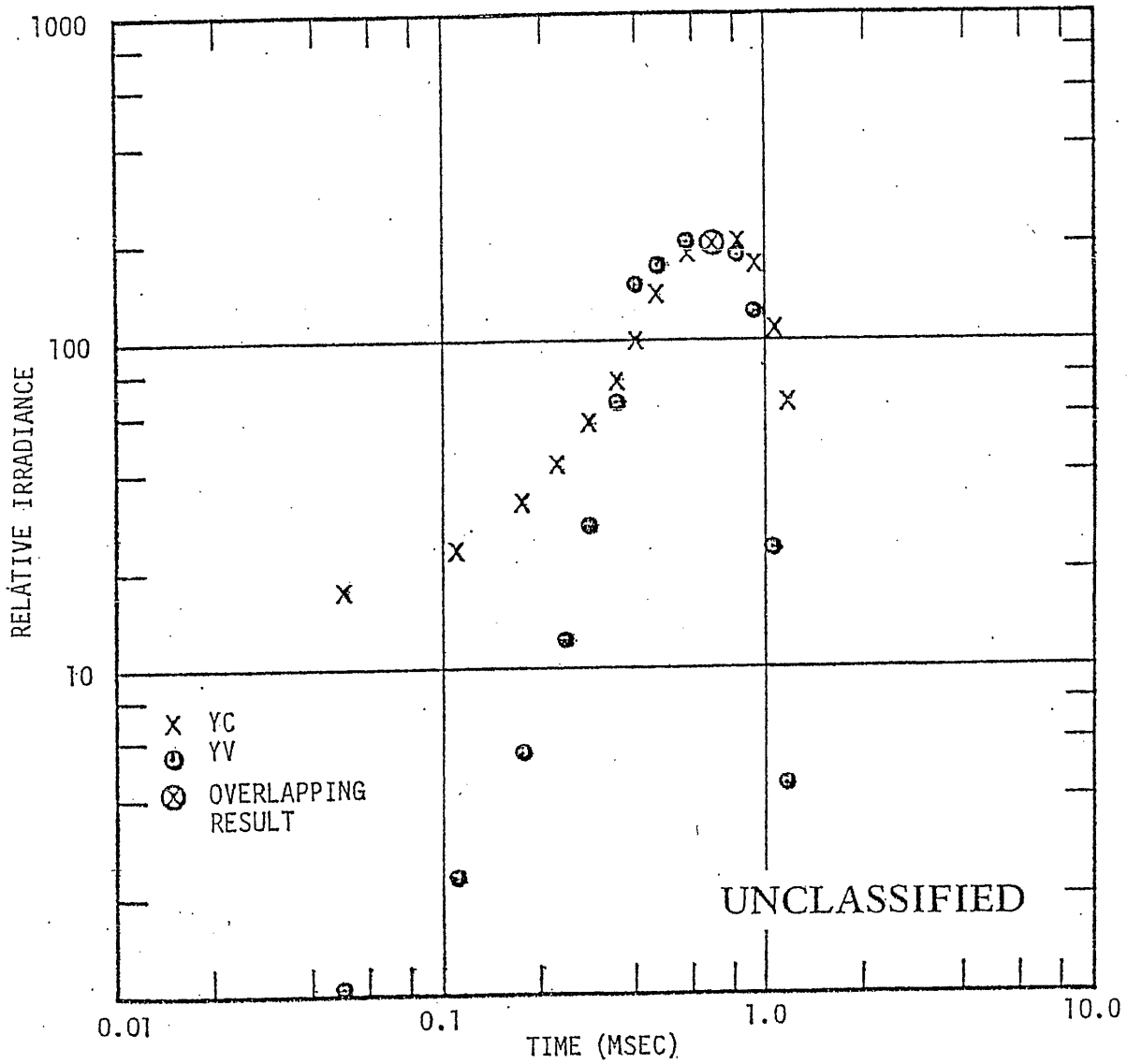


Figure 13 (U). Computed relative irradiance produced by a flat plate moving transverse to the optical axis and approaching from the YV sensor side

UNCLASSIFIED

~~SECRET~~

at late times the aspect angle of the plate, relative to the sensors, is more favorable. Results for two different rotations are shown in Figure 14. The effect is not large enough to make the computed curves fit the data for either peak.

(U) It is also possible to rotate the plate as it moves in front of the sensors. We have not performed any calculations for rotating plates. Based on irradiances computed for plates at different, fixed angles relative to the sensor plane, we do not believe that time-dependent rotation of the plate will produce agreement with the data for either peak.

3.2.3 TRAJECTORIES PARALLEL TO THE OPTICAL AXIS

(U) We assume that the plate moves in the x direction, along a line of constant y and z . Typical results are shown in Figures 15 and 16. The results in these figures are adjusted to fit the leading edge of the second peak in the YC data. The physical situation for these cases is that the plate approaches the satellite from above, and moves rather suddenly into the field of view as it passes the satellite. The late-time fall-off of computed irradiance is proportional to the inverse square of time, as the plate recedes from the satellite at nearly constant aspect angle. Because the time scale associated with the second peak is longer, velocities required for the plate are lower, of order 100 m/sec.

(8) In addition to seeing whether the YC data for the second peak can be reproduced, we are also interested in the difference between the YC and YV data for the second peak. In order to maximize the difference in viewing angles between each sensor and the plate, we put the plate trajectory very close to the satellite. For the case shown in Figure 15, the equations of the plate trajectory are

$$y = -0.154, \quad z = 1.0$$

(8)

~~SECRET~~

UNCLASSIFIED

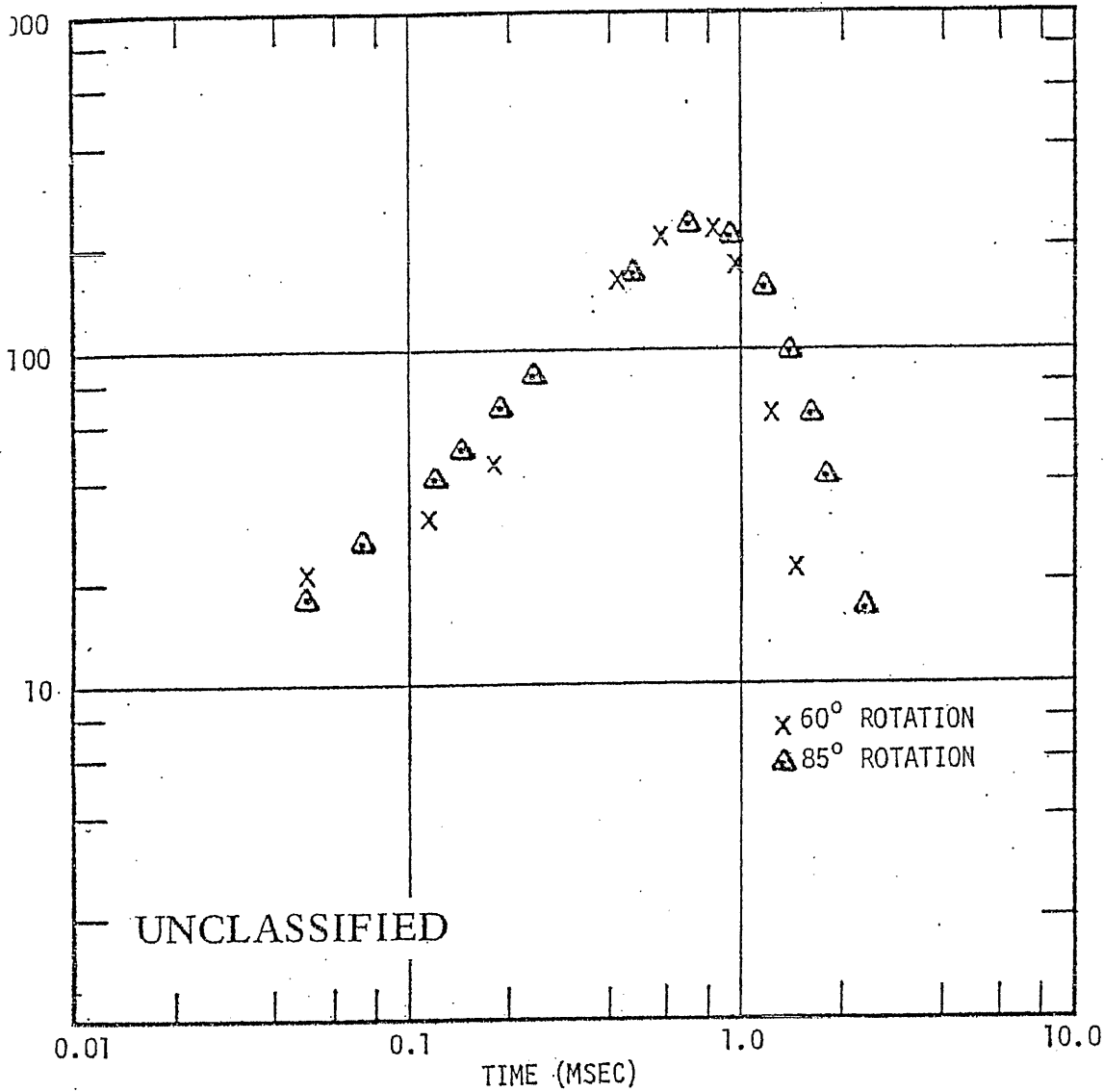


Figure 14 (U). Computed relative irradiance produced by a flat plate moving transverse to the optical axis, showing the effect of constant plate rotation

UNCLASSIFIED

UNCLASSIFIED

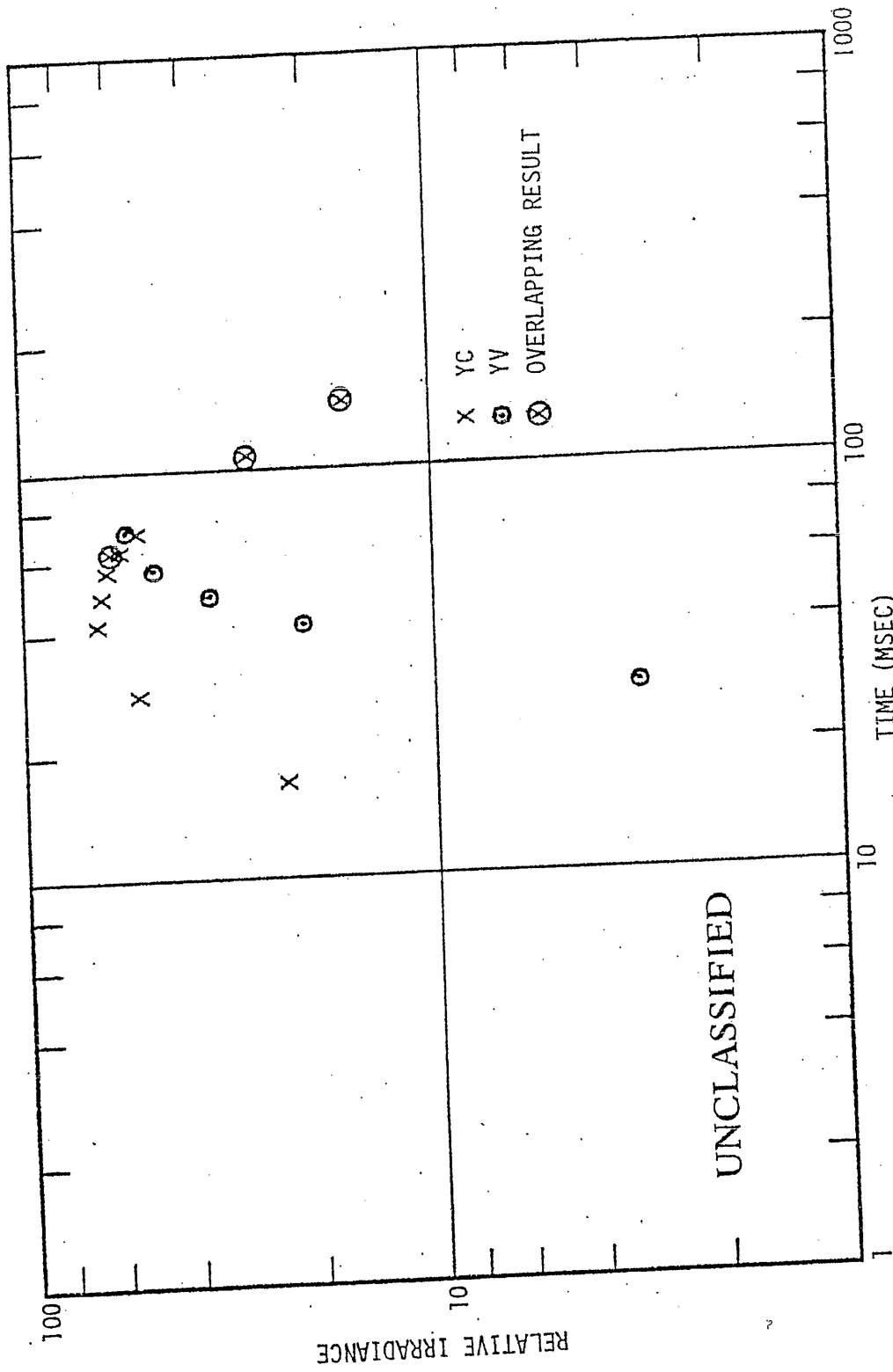


Figure 15 (U). Computed relative irradiance, 18 to 150 msec, for a flat plate moving parallel to the optical axis along a trajectory given by Equation 8

UNCLASSIFIED

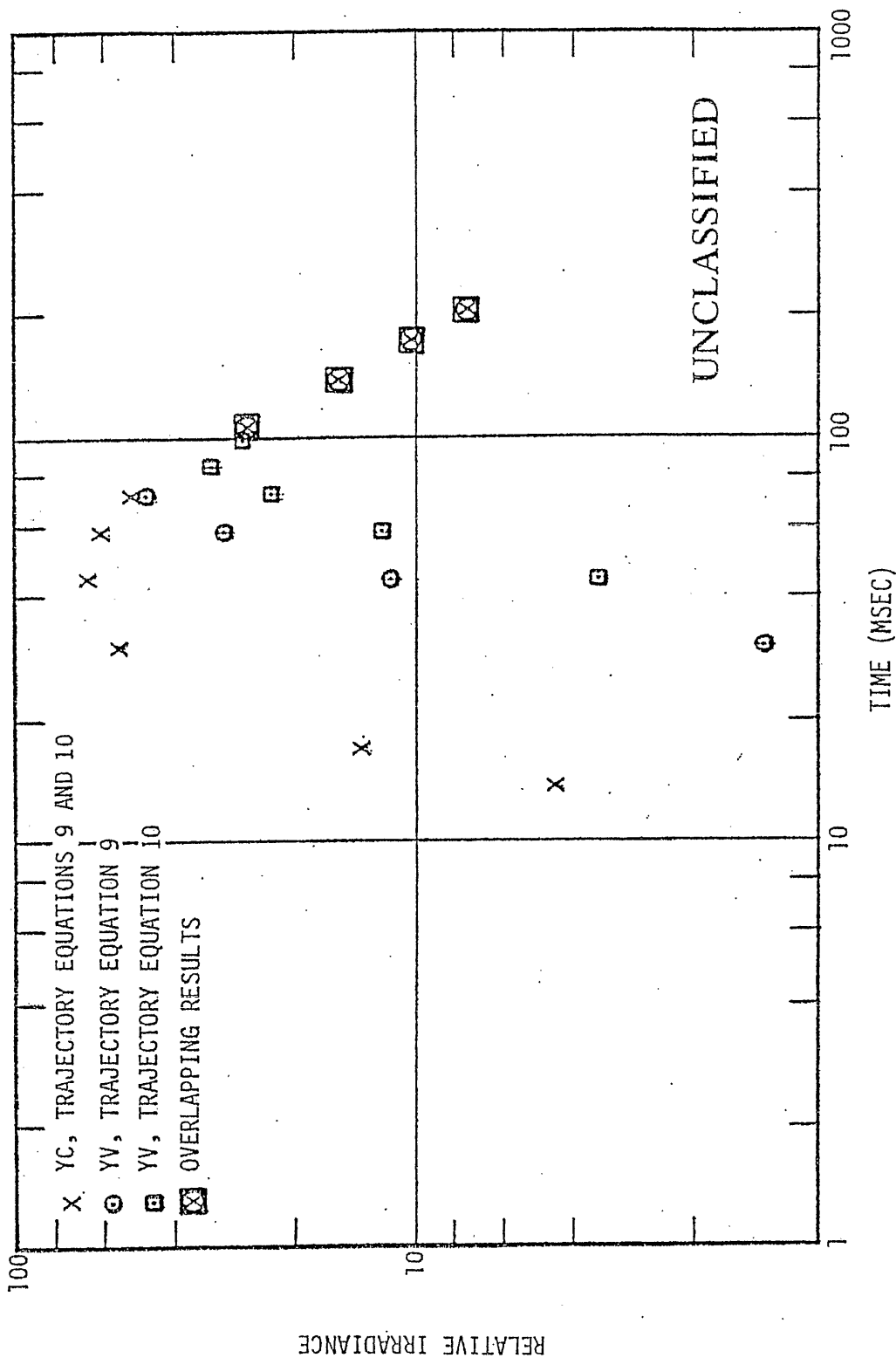


Figure 16 (U). Computed relative irradiance for a flat plate moving parallel to the optical axis along a trajectory given by Equations 9 and 10

~~SECRET~~

In other words, the plate emerges directly behind the YV sensor at a distance of 1 m. For the cases shown in Figure 16 one trajectory has equations

$$y = +0.3, \quad z = 1.0 \quad (9)$$

This trajectory has the plate emerging on the +y side of the YC sensor. The other trajectory has equations

$$y = +1.165, \quad z = 0 \quad (10)$$

On this trajectory the plate emerges at the same radial distance from the YC sensor as it does on the trajectory given by Equations 9. However, it is farther away from the YV sensor.

(8) Considering first the YC sensor results, we see that the agreement with YC data is not bad. The late-time, inverse square decay of the computed irradiance is a little fast. It is possible that the agreement could be fine-tuned by introducing some rotation of the plate into the calculation.

(8) It is clear from Figures 15 and 16 that we have no success simultaneously explaining the YC and YV data on the second peak, regardless of where we put the trajectory. When the trajectory is designed to put light on the YV sensor as early as possible (Equations 8) the YV amplitude is too large, relative to the YC amplitude. When the trajectory is moved away from the YV sensor, in order to reduce the peak YV amplitude, the time at which the YV amplitude peaks is too late.

(8) These results could be altered a bit by rotating the plate so that the aspect angle is more favorable for the YC sensor than for the YV sensor. However, nothing approaching the required peak irradiance difference between the two sensors can be achieved.

~~SECRET~~

~~SECRET~~

(U) Figure 17 shows an attempt to fit the data for the first peak with a flat plate moving parallel to the optical axis. The trajectory is given by Equations 8. The results are adjusted to give the best fit to the leading edge of the YC data. The required velocity of the plate is 8000 m/sec.

~~(S)~~ Again, the fit to the YC data is not bad, although the leading edge of the pulse is fit better with a transverse trajectory, and the fit to the YV data is poor. Movement of the trajectory away from the YV sensor makes the fit worse.

3.2.4 CONCLUSIONS

~~(S)~~ We conclude from this work that if one is willing to accept factor-of-2 accuracy, the YC data can be explained in terms of a pair of flat plates, behaving as "Lambert's Law radiators," that move on trajectories normal to the sensor optical axis with specific velocities and spacing. We also conclude that the YC and YV data are not simultaneously explained in these terms.

~~(S)~~ It appears to us that a simultaneous explanation of the YC and YV data requires introduction of source surface irregularity, and some degree of specularly in the reflectivity of the surface. Sources with these properties are considered in the next section.

~~SECRET~~

UNCLASSIFIED

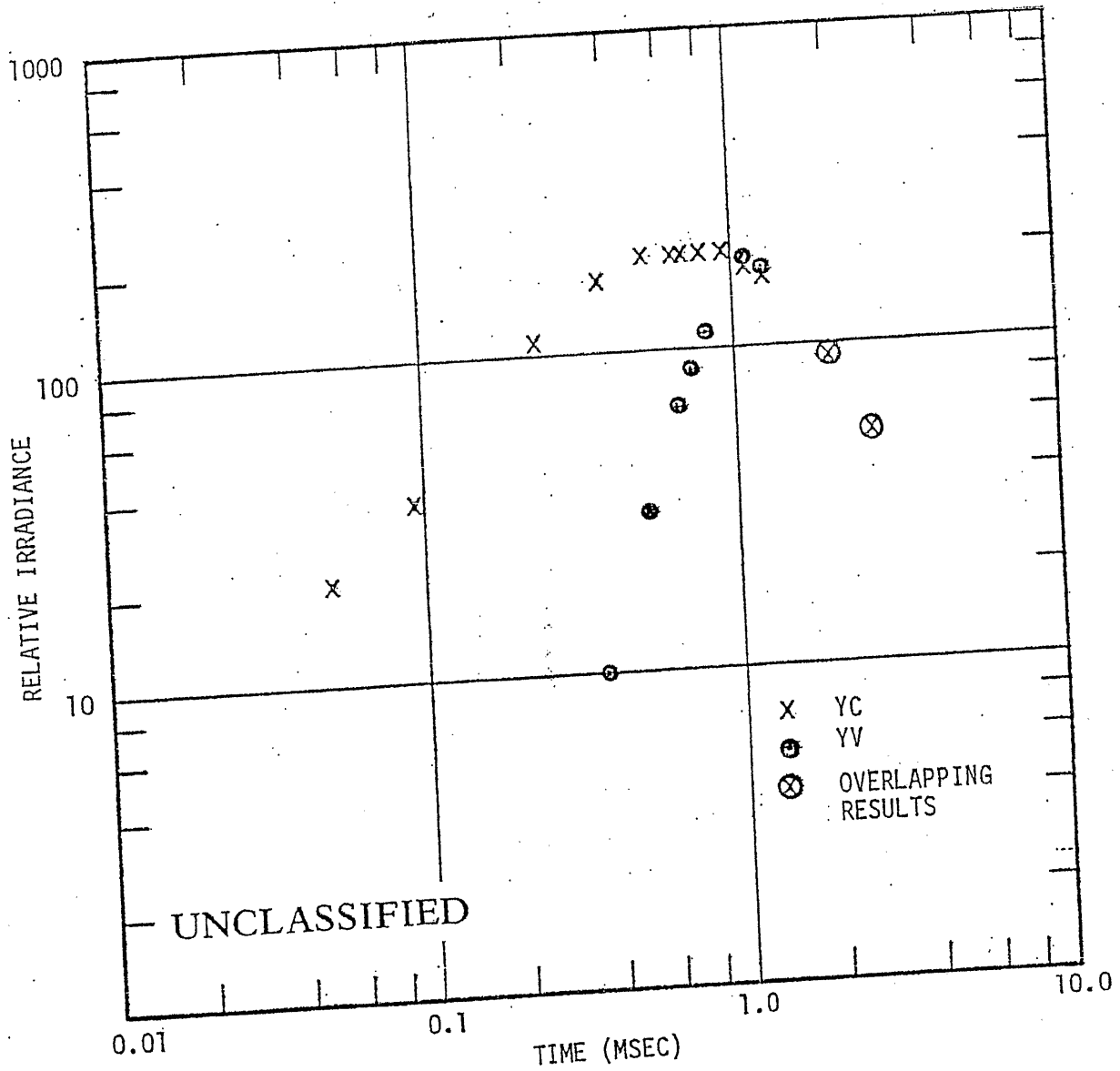


Figure 17 (U). Computed relative irradiance, 50 μ sec to 2.5 msec; for a flat plate moving parallel to the optical axis along a trajectory given by Equation 8

UNCLASSIFIED

~~SECRET~~

3.3 SINGLE OBJECT STUDY

3.3.1 SUMMARY AND CONCLUSIONS

~~(S)~~ This section contains the major results of a study intended first to demonstrate that, without violation of physical law, a single passive object may produce bhangmeter data which closely mimics a nuclear explosion, specifically Event 747; second to discover any restrictions which must be imposed upon the characteristics and trajectory of such an object; and finally to assess the credibility of such an object being responsible for the observed data, if possible.

~~(S)~~ Major conclusions of this single object study are:

1. A class of objects and associated trajectories are conceivable which would have produced the observed data, had such an object been present.
2. All members of this class are highly contrived objects with significant structural features matched to restricted trajectory; none is as simple as a sphere, rod, plate, or other common shape.
3. In the absence of a history of very many (10^2 to 10^6) multiple pulse events with nuclear-like rise to first maximum*, but of obviously non-nuclear origin, a single-particle produced curve closely resembling a nuclear signature is most difficult to credit.

* (U) To the authors' knowledge, exactly one such event exists. Members of the collection known as the "zoo" all fail to meet the criterion of a nuclear-like rise to first maximum.

~~SECRET~~

3.3.2 MAJOR RESTRICTIONS ON ANY SINGLE OBJECT/TRAJECTORY

3.3.2.1 Assumptions

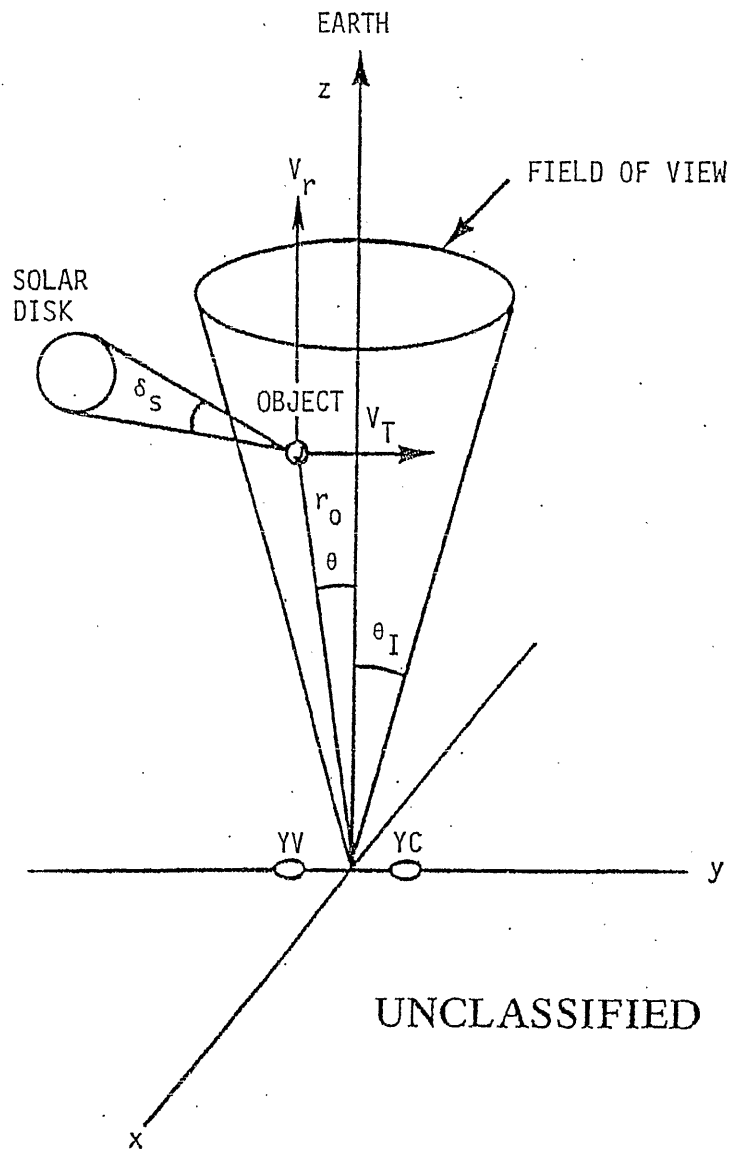
(U) It is assumed that instrumental response is normal and reasonably represented by response curves shown in Figure 11. By "normal" we mean that (1) amplitude response within 10° to 15° of the axis is accurate within about 20 to 30 percent relative to nearby angles of both instruments, (2) amplitude response is stable within 20 to 30 percent for the time required to record Event 747, and (3) instrumental response is axially symmetric within about 1° for both instruments.

3.3.2.2 Coordinates

~~(S)~~ The coordinate system is illustrated in Figure 18. The origin is centered midway between the two silicon detectors, which lie on the y axis separated by distance $d = 0.3$ m. The z axis points away from the satellite surface on which the detectors lie, toward earth to any accuracy which concerns us. A sharp drop in sensitivity occurs at polar angle $\theta_I \approx 10^\circ$ to 15° (from Figure 11). The sun is at polar angle $\theta_S \approx 70^\circ$; solar azimuth appears unimportant. The solar disk subtends angular diameter $\delta_S = 0.5$ degrees $= 8.73 \times 10^{-3}$ rad. A rigid, passive, sunlit object which is assumed to produce the entire signal observed by both detectors is located at polar angle θ and spherical polar radius r_o . The object moves with velocity component transverse to the field of view (parallel to the x-y plane) V_T and component parallel to the z axis, V_r .

(U) When the object is considered to be very near the x-y plane, one must evaluate detector sensitivity utilizing a temporary coordinate system centered on the individual detector.

UNCLASSIFIED



UNCLASSIFIED

Figure 18 (U): Coordinate system for single object study

UNCLASSIFIED

3.3.2.3 Restrictions

- (S)
1. The object must reach a point close to the center of the field of view of both instruments without being detected. If the object's polar angle at the moment a detector triggers is denoted by θ_o , then

$$\theta_o \leq 6^\circ \quad (11)$$

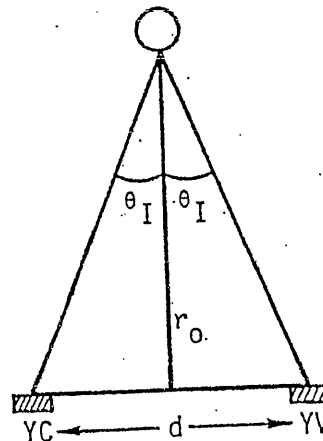
(S) This restriction follows from the fact that the first pulse shape and amplitude are consistent with nominal center-of-field sensitivities of the two bhangmeters. The consistency of the two bhangmeters' first pulse measurements also supports the basic assumption on which this study of non-nuclear sources rests, that instrumental response is near nominal.

- (S)
2. At the time of the first pulse, the object must be farther from the detectors than about 1.5 m.

(S) This restriction also follows from consistency of both first pulse records. In order to be within 6° of the center of the field of view of two instruments which are separated by distance, d , one must have

$$r_o \geq \frac{d}{2 \tan \theta_I} = \frac{0.3 \text{ m}}{2 \tan 6^\circ} \approx 1.42 \approx 1.5 \text{ m} \quad (12)$$

The geometry is illustrated in the sketch.



~~SECRET~~

~~(S)~~ 3. The object must be within about 30 meters of the detectors.

~~(S)~~ This important restriction follows from the facts that (1) second pulse timing and shape are different as recorded by the two detectors and (2) the object are known to have been near the center of the field of view of both detectors at the start of the record.

~~(S)~~ Figure 19 compares second pulse apparent irradiance for the two detectors. "Apparent irradiance" means that nominal calibrations for center of field sensitivity have been applied to the data. No simple trajectory through the sensitivity pattern of Figure 11 can reproduce the data (i.e., no far field trajectory). The curve labeled $3 \times YV$ shows that no single scaling of relative sensitivity could produce the observed data*.

~~(S)~~ Since no reasonable far field trajectory can explain differences in second pulse timing and shape, we conclude that irradiance on the two detectors is different. This means that if the object is distant then the object has optical properties capable of differently illuminating two points 0.3 m apart. The sharpest possible difference in illumination would arise if the object were capable of focussing a perfect image of the solar disk on the satellite detector plane. If the two detectors are to be illuminated to a different extent then the solar disk image must be comparable to, or smaller than,

* (U) If satellite spin period were comparable to signal duration a rather complex apparent trajectory would be conceivable. However, this is not the case; satellite spin period is 64 seconds compared to signal duration of 0.3 seconds.

~~SECRET~~

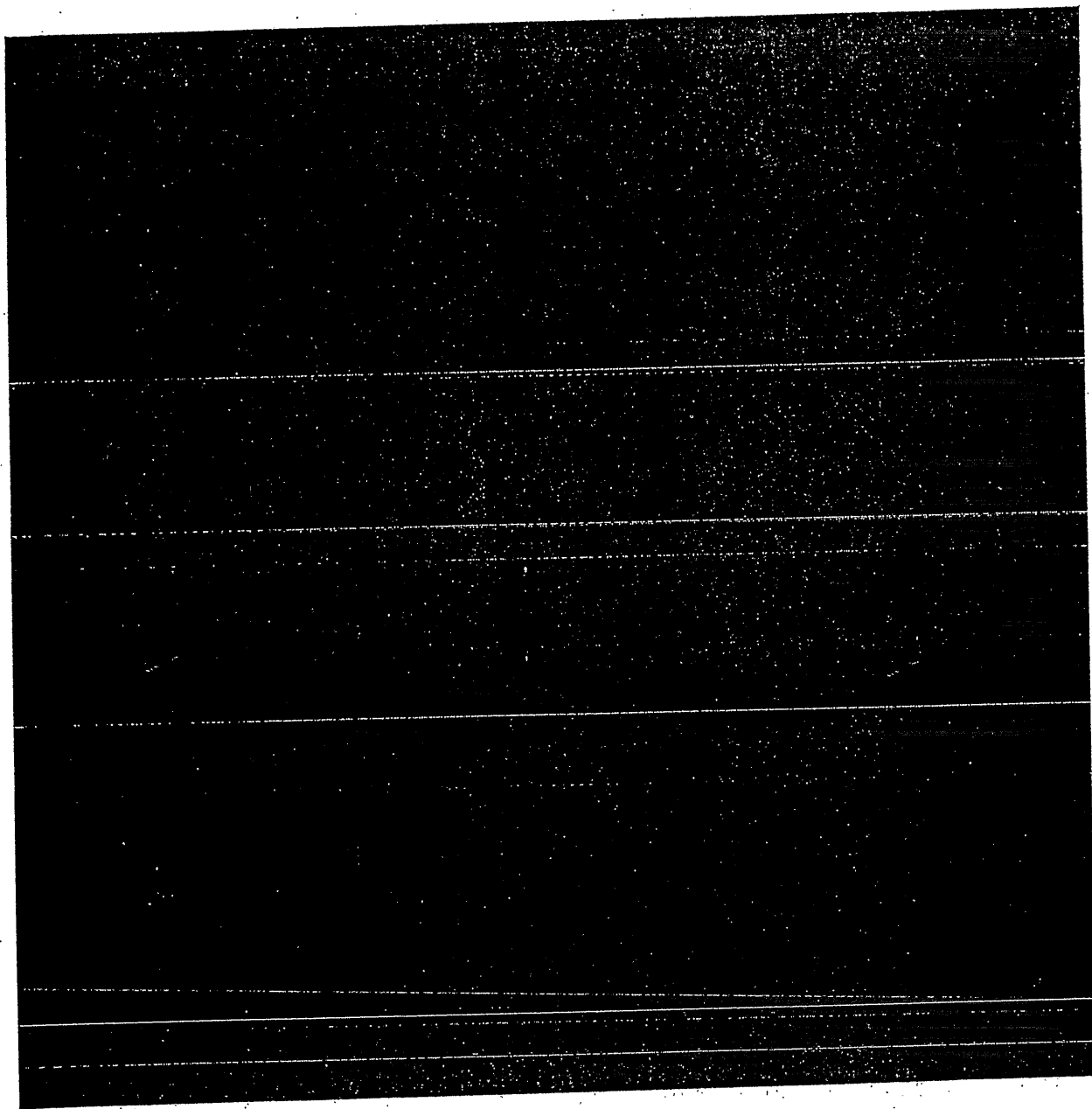


Figure 19 (U). Second pulse irradiance, showing different instrument responses

~~SECRET~~

the spacing between detectors. From Figure 20 one sees that, for a distant source like the sun, the best possible image is obtained by placing the object at a distance equal to its focal length. The image size is $r\delta_s = d$, where r , in this case the focal length, f , is the distance of the object, δ_s is the angular diameter of the solar disk (9×10^{-3} rad), and d is the distance between detectors. Then

$$r = d/\delta_s = 0.3 \text{ m}/9 \times 10^{-3} = 30 \text{ m} \quad (13)$$

If the image is imperfect, as it must be to yield the observations, then the object must be even closer. Therefore we find the important conclusion that

$$r < 30 \text{ m} . \quad (14)$$

4. The angular velocity of the object across the field of view is given by the ratio of transverse velocity to distance.

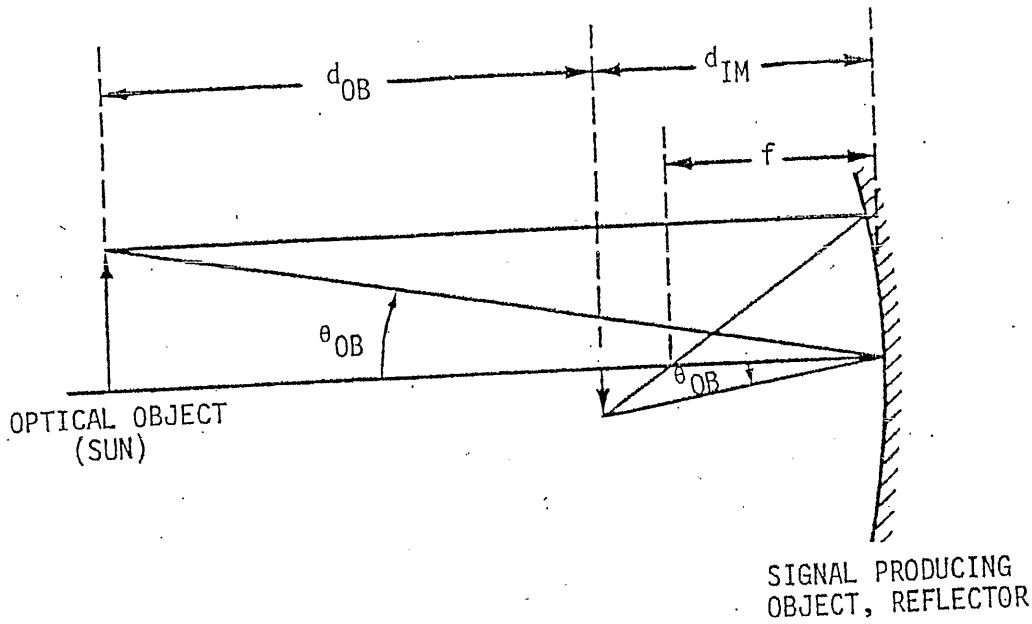
$$V_T/r \approx 0.5 \text{ sec}^{-1} \quad (15)$$

This restriction is a consequence of the requirements that, (1) according to the sensitivity curve, Figure 11, the object cannot be seen beyond a polar angle of about $\theta_I = 10^\circ$, or 0.16 rad, (2) it must start near the center of the field of view, and (3) it disappears in about 0.3 sec according to Figure 19. Then

$$\frac{V_T}{r} \sim \frac{\theta_I}{\tau} = \frac{0.16 \text{ rad}}{0.3 \text{ sec}} \sim 0.5 \text{ sec}^{-1} \quad (16)$$

~~SECRET~~

UNCLASSIFIED



- IMAGE SIZE = $d_{IM} \theta_{OB}$
- IF $d_{OB} \rightarrow \infty$
 $d_{IM} \rightarrow f$
IMAGE SIZE $\rightarrow f \theta_{OB}$
- ABERRATIONS ADD STRUCTURE BY SPREADING IMAGE

UNCLASSIFIED

Figure 20 (U). Fundamental limitation on irradiance variability

UNCLASSIFIED

~~SECRET~~

- (S) 5. The first pulse must be produced by a highly specular reflection from a facet on the object; it must be a glint.

(S) The duration and rise time of the first pulse are both $\sim 10^{-3}$ sec. There are three possibilities,

(a) $V_T/r \sim \theta_I/10^{-3} = 160$. This can't be true since (i) we already know V_T/r and (ii) if so, no second pulse would have occurred because the object would be out of the field of view.

(b) It is a diffuse surface which produces the signal by rotation. A diffuse surface must turn through about 90° , or $\pi/2$ radians, to bring its signal to maximum. Then the angular velocity of spin would be

$$\omega_s \sim \frac{\pi}{2} / 10^{-3} \text{ sec} \sim 1500 \text{ rad/sec}.$$

This is not the case; if it were true one would see more signal structure with 1 msec time scale than just the first pulse.

(c) Finally, it may be a specular surface. Then the structure is controlled by the angular size of the sun's image and

$$\omega_s \sim \frac{\delta_s}{2} / 10^{-3} \text{ sec} \approx 5 \text{ rad/sec}$$

This is a reasonable number which does not conflict with any known characteristic of the signal. Thus we conclude that the first pulse is due to a highly specular facet, tailored to mimic a bomb.

- (S) 6. The spin rate of the object about one axis (axis 1) is

~~SECRET~~

~~SECRET~~

$$\omega_{s1} \sim 5 \text{ rad/sec} .$$

(17)

7. At least the first exposed portion of the surface responsible for the second pulse must be fairly specular. Otherwise, the object must rotate about axis 2, perpendicular to axis 1, at a rate of

$$\omega_{s2} \sim \frac{\pi}{2} / 15 \times 10^{-3} \approx 10^2 \text{ rad/sec} ,$$

to create a gap in illumination of about 15 msec duration and a rise time for the second pulse of some tens of milliseconds. This can't be so, for it would cause structure with 10 msec characteristic time throughout the second pulse. On the other hand, a specular surface requires a spin rate of only

$$\omega_{s2} \approx \delta_s / 15 \times 10^{-3} \sim 0.5 \text{ rad/sec} .$$

(18)

This represents a minimum value of spin about the second axis.

8. The spin rate about the second axis is

$$0.5 \text{ rad/sec} \leq \omega_{s2} \leq 20 \text{ rad/sec} .$$

(19)

The lower limit was found above. The upper limit arises from the lack of fine structure in the second pulse, of duration $\tau = 0.3 \text{ sec}$,

$$\omega_{s2} \leq 2\pi/\tau \sim 6/0.3 = 20 \text{ rad/sec} .$$

9. The velocity component parallel to the z axis is limited to

$$|V_r| / r_0 \leq 6 \text{ sec}^{-1} .$$

(20)

~~SECRET~~

~~SECRET~~

Roughly, the signal falls a factor of ten while time increases a factor of ten after second maximum. Then, the r^2 law requires,

$$r(0.3 \text{ sec}) \approx 3 r(0.03 \text{ sec})$$

But, for practical purposes, $r(0.03 \text{ sec}) = r_0$, so

$$V_r \leq \frac{r(0.3 \text{ sec}) - r_0}{\tau} \approx \frac{2r_0}{0.3 \text{ sec}} \approx 6r_0 \text{ sec}^{-1}$$

then $V_r/r_0 \approx 6$.

- (9) 10. The main surface cannot have a simple structure. The second pulse requires unequal illumination of the two detectors not explicable by any trajectory of a surface with constant curvature through the sensitivity patterns of the detectors.

3.3.3 EXAMPLES OF POSSIBLE OBJECTS AND ASSOCIATED TRAJECTORIES

(U) The previously listed ten restrictions apply to any single rigid object which could conceivably produce the observed bhangmeter signals. Except for requirement (10), which depends upon a trial and error search through the sensitivity patterns, it is hoped that the restrictions are evident based on physics and the main characteristics of the observed signal.

(U) The following is a brief discussion of four examples, intended to illustrate the sorts of objects which meet the above requirements. Each example entails a number of restrictions additional to the above ten, along with its own set of tradeoffs among some of them. The first three are appropriate to distances of passage greater than about 5 meters, and the last to closer distances. There are undoubtedly many more possible types of objects in addition to these four, but they must all be as contrived and restricted as these.

~~SECRET~~

UNCLASSIFIED

(U) In general, all types are equal with regard to the first maximum, which can only be explained by a carefully tailored glinting facet which has no relation to the remainder of the object. Thus, all allowable solutions are tantamount to attaching a second object to the first.

Example 1. Facets on a Plate

(U) This object is possibly the most contrived but conceptually the easiest. It is composed of a large number of facets shielded from view of the detectors until the appropriate time for second maximum and is conceptually illustrated in Figure 21. The entire structure of both detectors' response can be constructed by judicious choice of facets. One thinks of a crystal form similar to a snowflake.

(U) Only one thing must be shown to prove this general configuration possible. That is that the diffraction limit not be exceeded for appropriate intensity.

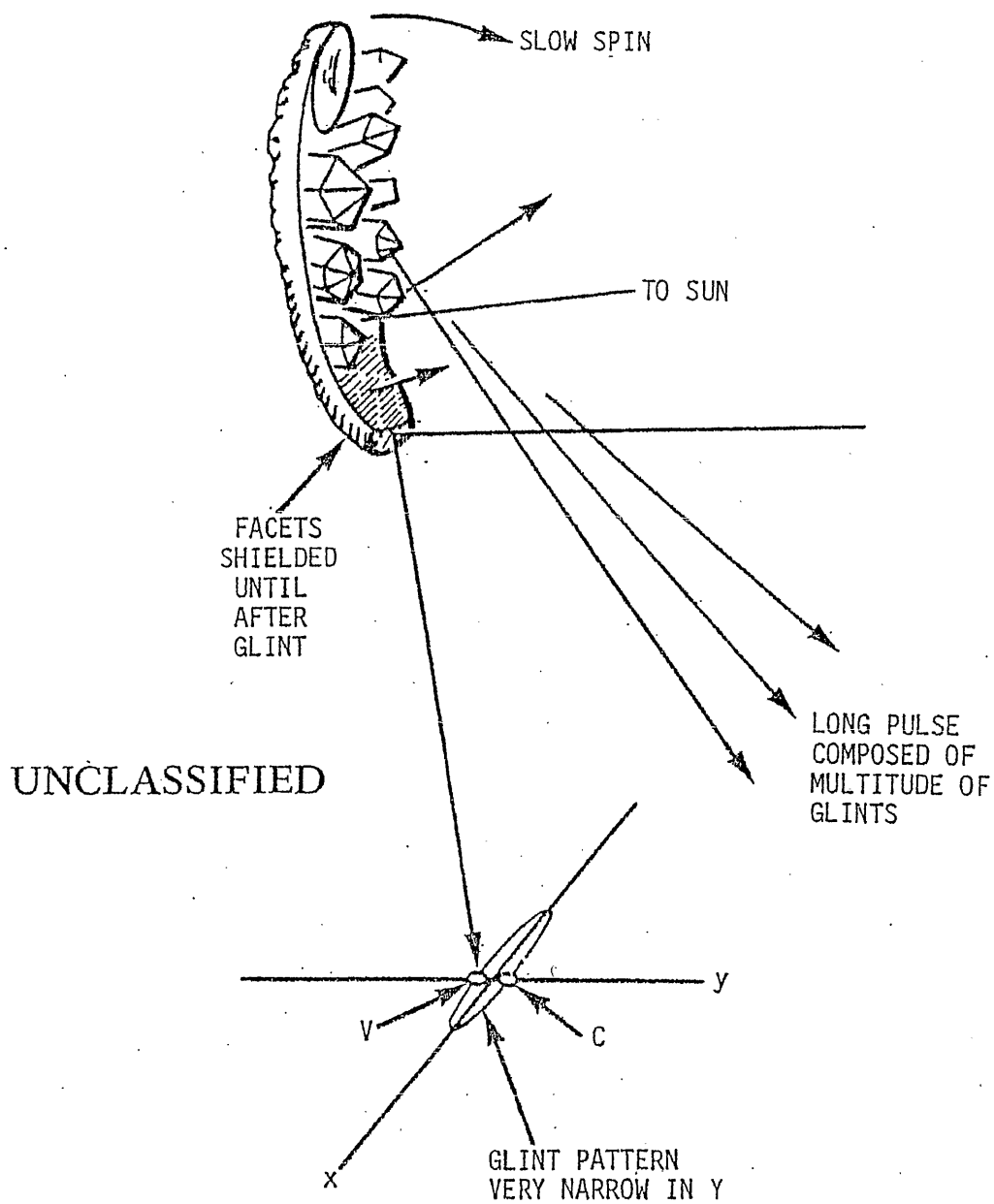
(U) Diffraction Limit. If the linear dimension of a facet is a_f , then to produce an image sufficiently well defined that the two detectors can see very different levels of illumination, the angle subtended by the two detectors, θ_d , must exceed the diffraction limit,

$$\theta_d = \frac{\lambda}{a_f} < \frac{d}{r} \quad (21)$$

(U) Taking $\lambda = 6000\text{\AA}$ as typical and $d = 30$ cm, one can solve for

$$\frac{a_f}{r} > \frac{\lambda}{d} = \frac{6 \times 10^{-5}}{30} = 2 \times 10^{-6} \text{ rad} \quad (22)$$

UNCLASSIFIED



UNCLASSIFIED

Figure 21 (U). Multifaceted object

UNCLASSIFIED

UNCLASSIFIED

(U) We note that, since r is less than 30m, we can stand a_f as small as

$$a_f \sim 2 \times 10^{-6} r \sim 6 \times 10^{-3} \text{ cm} \quad (23)$$

(U) An array of 10^3 such facets need only have diameter

$$D \geq 2\sqrt{10^3} a_f = 0.4 \text{ cm} \quad (24)$$

These are quite reasonable as dimensional lower limits.

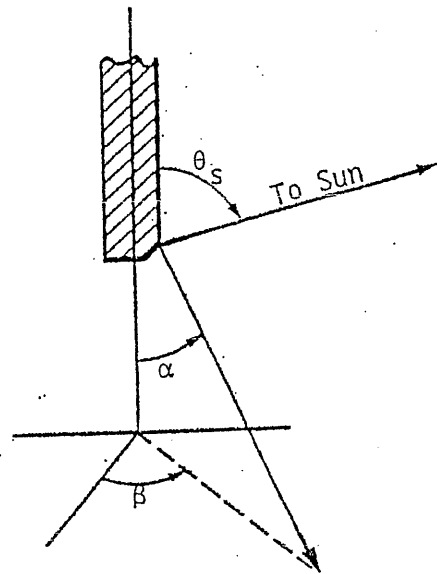
(U) Radiant Intensity Formulation.

The intensity at a detector is conveniently described in a coordinate system defined by the object as indicated in the sketch.

$$I = \frac{F_s R \sigma G S}{4\pi r^2} \quad (25)$$

where I (watts/cm²) is irradiance at the detector, r is distance to the detector, F_s is solar irradiance, R is mean reflectivity (or albedo) of the surface, σ is the physical cross sectional area of the surface in question (a facet or a side), S is detector sensitivity at detector polar angle θ , and G is a gain function, such that

$$1 = \frac{1}{4\pi} \int_0^{2\pi} d\beta \int_0^\pi \sin\alpha d\alpha G(\alpha, \beta, \theta_s)$$



UNCLASSIFIED

(U) For an isotropic scatterer, $G = 1$ always. For our purposes we can drop θ_s as a variable since it will not need to be explicitly considered.

(U) Implication for Facet Dimension. Typical values are:

$$I = 2 \times 10^{-9} \text{ watts/cm}^2$$

$$R = 0.5$$

$$G \leq \frac{8}{\pi \delta_s^2} = 2.9 \times 10^4$$

$$\delta_s = 9.3 \times 10^{-3}$$

$$F_s = 0.14 \text{ watts/cm}^2$$

$$S < 1$$

(27)

(U) Substitution into Equation 25 yields

$$\frac{\sigma}{r^2} > 1 \times 10^{-11} \quad (28)$$

So

$$\frac{a_f}{r} \sim \sqrt{\frac{\sigma}{r^2}} > 3.5 \times 10^{-6} \quad (29)$$

which satisfies Equation 22. Thus, no problem exists in imagining facets of ordinary material which produce both the observed level of radiance and the required variation of radiance.

UNCLASSIFIED

(U) The ratio of peak intensities of the first and second pulse is of order 1 for either detector.

$$\frac{I_1}{I_2} = \frac{R_1 \sigma_1 G_1 S_1}{R_2 \sigma_2 G_2 S_2} \sim 1 \quad (31)$$

(U) One would like R_1 and R_2 to be similar and S_1 must be nearly equal to S_2 since the object can't have moved very far in the first 40 msec. But the ratio of pulse durations requires that σ_2 be greater than σ_1 , in fact nearly 10^2 times as big.

$$\sigma_2 \sim 10^2 \sigma_1 \quad (32)$$

(U) The only simple option to maintain the measured intensity ratio is to reduce G_2 relative to G_1 . The gain from an object with circular cross section can be as large as

$$G \leq \frac{\pi}{\theta_s} \sim 7 \times 10^2 \quad (33)$$

so it is possible that $G_1 \approx 100 G_2$. For normal reflectivities the object should be small, from Equation 29 the dimensions need be only about 0.5 cm diameter by 5 to 50 cm length at the extreme value of r to produce the required intensity and variations.

(U) This type object has the same problem as the first example in terms of a high optical quality first maximum facet. It has eliminated the problem of multiple facets which produce too-smooth variations, in favor of the problem of a rod bent at 90° having an orientation such that the top portion fails to trigger either detector prior to the glint. A sketch of such an object appears in Figure 22.

UNCLASSIFIED

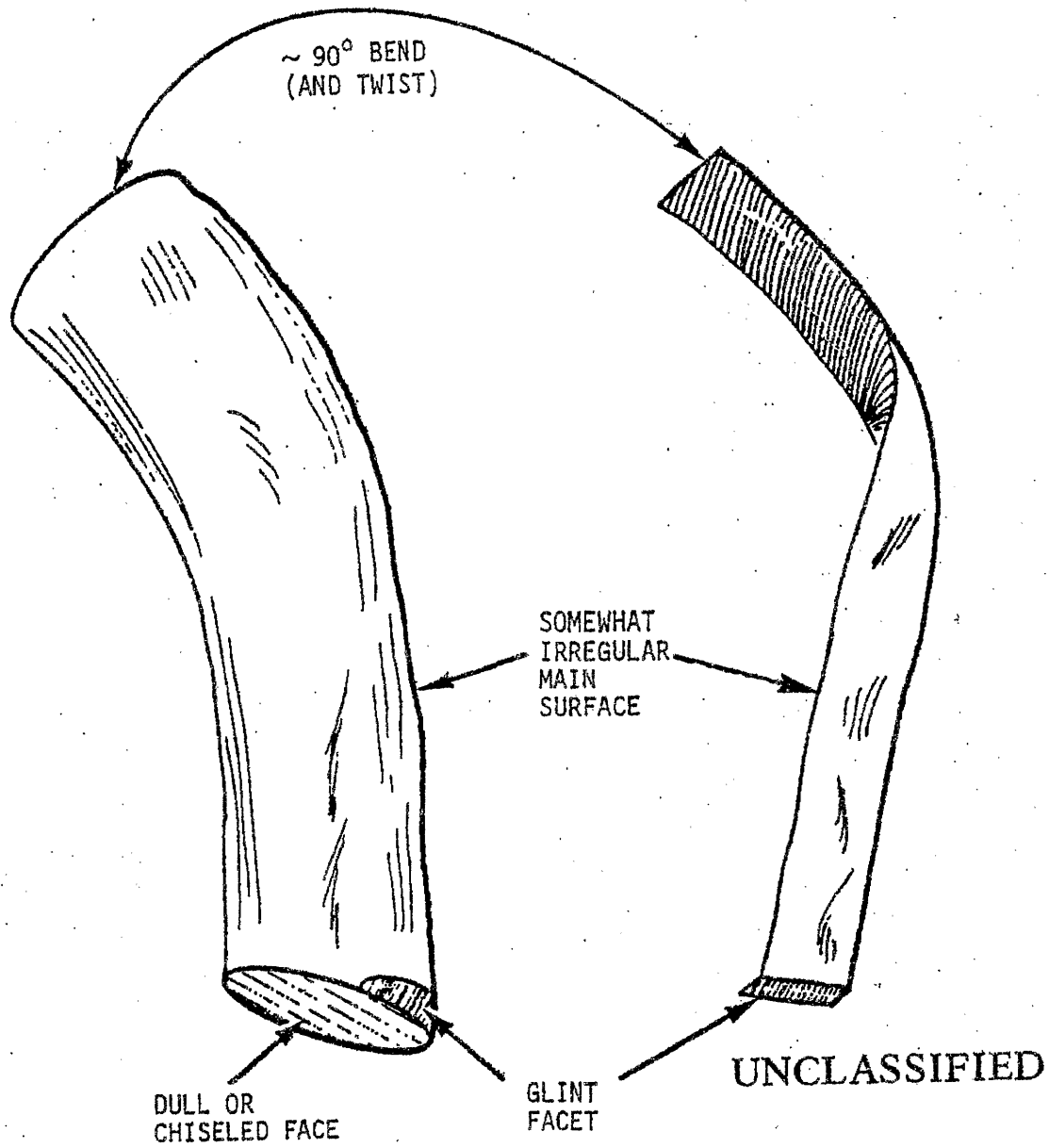


Figure 22 (U). Bent rod and helix cases

UNCLASSIFIED

UNCLASSIFIED

(U) Option 2A. One way out of this is to imagine a rod which somehow gently, so as not to produce a larger than required perturbation, grades from specular near the bottom into irregular Lambert's Law near the top. Now the rod need not be bent so much, just enough to expose areas with somewhat irregular optical properties (including imaging properties).

Example 3. Helix

(U) Another option is to replace the rod with a bent and twisted helix, illustrated in Figure 22. It can be flat with irregularities and the glint facet can be a sharply bent segment at the bottom. There is no intensity matching problem if it is bent. If it is specular and spins then it must be helical with pitch matched to spin. If it grades into semi-Lambert's Law reflection then the twist and most of the bend are unnecessary, as in Example 2A.

Example 4. Near Field Hemisphere

(U) The above examples produce the required variations in second maximum detector illumination by virtue of weak imaging features on their main surface. They all require very systematic features to delay the second pulse on YV and then to systematically keep it down relative to YC until the object drifts far enough out of the center of the field for the narrower field of view of YV to take over. Thus, many of the interesting features are produced by relatively tight requirements on surface but comparatively loose requirements on trajectory and initial position.

(U) An alternative approach is to imagine an object rather close to the detectors, so close that its trajectory carries it through a different

UNCLASSIFIED

portion of each detector's field of view. Then the variability might be caused by separate paths through the two detector sensitivity patterns.

(U) After much trial and error, the best case we have come up with is the object illustrated in Figure 23, moving on the trajectory shown in Figure 24 from the $t = 0$ position,

$$r_0 = 215 \text{ cm, at } V = 1.0 \text{ m/sec .}$$

(U) The θ, ϕ trajectory shown is the best compromise believed possible to minimize the need for an optically structured main surface.

(U) The component of velocity toward or away from the detector plane is unimportant provided it be not orders of magnitude greater than the velocity component in the plane of the detectors. The results are, however, sensitive to r_0 and the θ, ϕ trajectory.

(U) The object size is of the order of one millimeter. One dull patch on the main surface is necessary to chop off the YV maximum (or a patch to focus light on YC), as can be seen from Figure 25. In this figure the absolute irradiance required to produce each detector's signal for the chosen trajectory is compared. The difference in curves, and the raggedness of the YC curve beyond 100 msec is due to errors in naked eye graph reading for hand calculations. This part of the curve is in good agreement. It is only necessary to introduce one irregularity on the object, a smudge to reduce the YV maximum, or a focusing area to brighten YC.

(U) A nice feature of this case is that the delay in onset of the YV sensor second pulse can be attributed to the fact that the detectors are at substantially different angles from the object. Depending upon the direction

UNCLASSIFIED

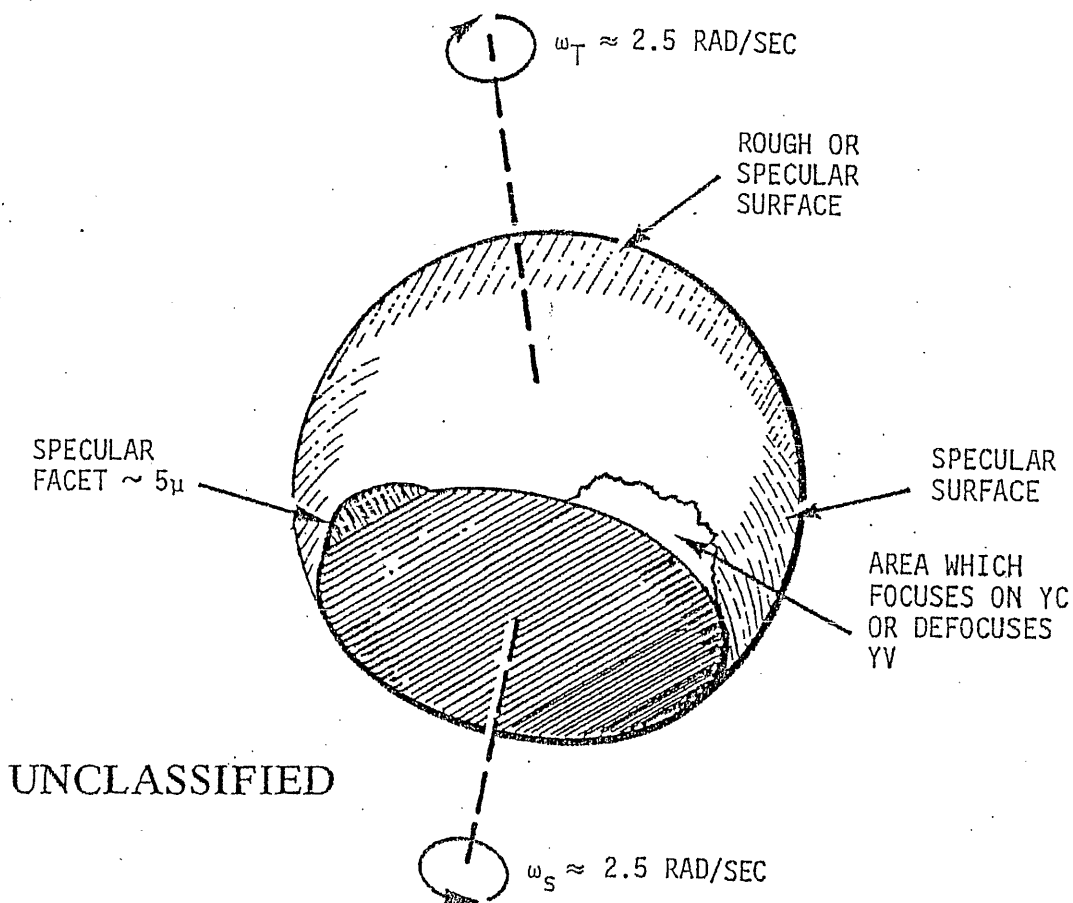


Figure 23 (U). Near field truncated sphere. Diameter $\sim 1 \text{ mm}$

UNCLASSIFIED

UNCLASSIFIED

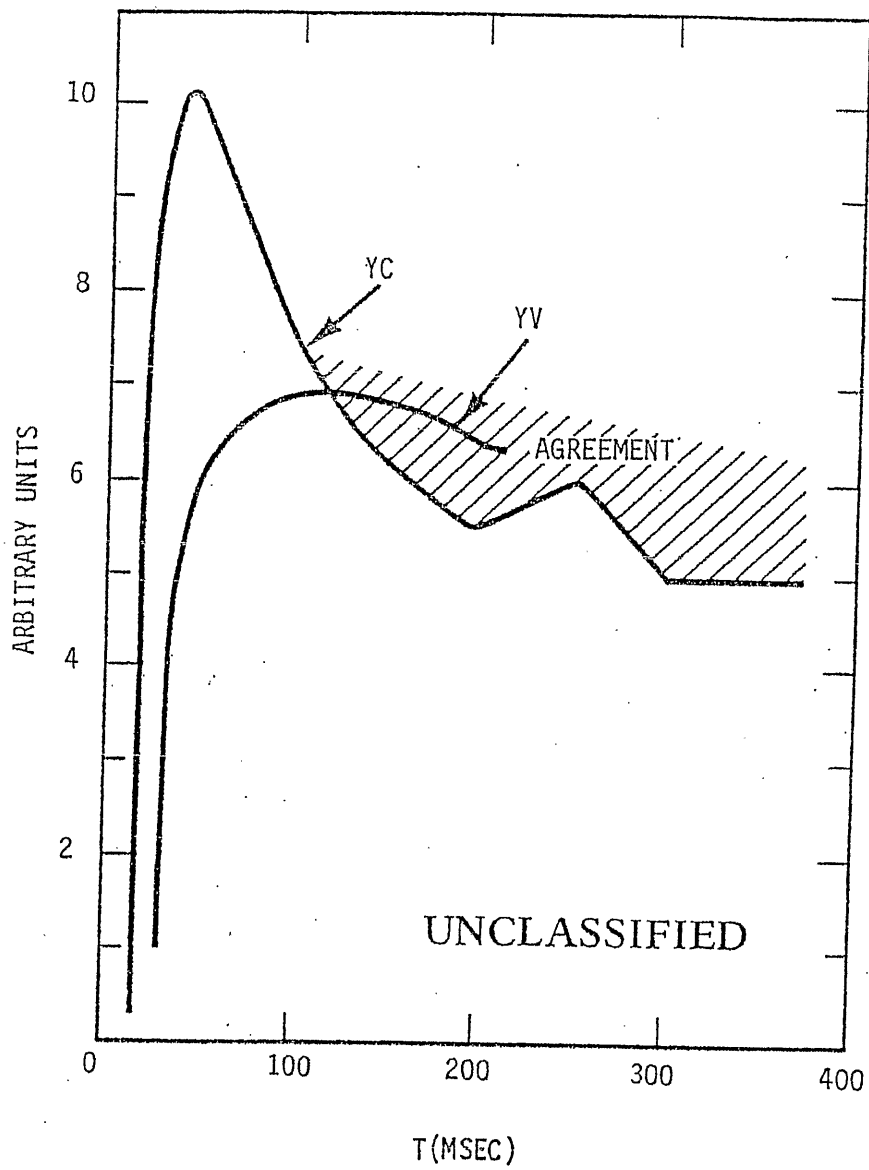


Figure 25 (U). Irradiance required on detectors from truncated sphere. Rise time difference due to object tumble. Early YC peak relative to YV requires surface structure

UNCLASSIFIED

~~SECRET~~

of tumble, a reasonable tumble rate, between $\omega = 0$ and $\omega = 5$ rad/sec, will account for the 10 to 20 msec delay in rise of the YV detector without introduction of an additional nonuniformity on the object.

3.3.4 CREDIBILITY

~~(S)~~ Subjectively, a reflection from an object similar to Example 4 seems to us to be the most likely non-nuclear explanation for the Event 747 data. However, it is the best of a very bad lot. The likelihood of finding an object with speed in the restricted range $1 \text{ m/sec} \leq V \leq 10 \text{ m/sec}$ in the immediate vicinity of the satellite seems remote indeed. The natural speed of objects spun off the satellite is 0.1 m/sec in the wrong direction; how to ten-fold their velocity while bringing them around the satellite so they can be seen by the detectors is hard to imagine. This problem is treated in detail in Appendix A. The natural relative speed of an object in similar orbit is of order 10^3 m/sec. Cislunar and solar system associated speeds are even higher.

~~(S)~~ If one can surmount this difficulty, then a very bomb-like signal must be produced. It is not incredible that such could happen, as has been shown. What is incredible is that a bomb-like signal should be among the first such signals observed. If there were historical records of 10^6 , or perhaps even 10^2 events consisting of bomb-like first maximum followed by second maximum at the wrong time, with the wrong intensity, duration, or shape, then we could more readily believe Event 747 to be a false alarm. But that is not the case, and we must regard a single particle origin for this signal as conceivable, but so improbable as to stress reason.

~~SECRET~~

UNCLASSIFIED

APPENDIX A

(This Appendix is Unclassified)

LOCAL SOURCE ORBITAL CONSIDERATIONS FOR A SINGLE OBJECT

Given the tight restriction on velocity of object relative to satellite of ~ 10 m/sec compared to VELA orbital velocity of about 10^3 m/sec, and especially the restriction on proximity, 10 m distance out of 10^8 m orbital radius, the most natural source for the object is the satellite itself.

So far two classes of local source have been suggested for which orbital considerations have importance, a particle somehow ejected from the satellite into a similar earth orbit and a particle orbiting the satellite under electrostatic forces. In the following we conclude that neither class of object is credible.

A.1 Earth Orbit

For a central force field

$$\frac{d^2}{dt^2} \vec{r} = - \frac{K}{r^2} \hat{r} \quad (A1)$$

where t represents time, \vec{r} the vector position in a coordinate system with origin at the center of force, K a constant*, and \hat{r} a unit vector in the radial direction.

* In the case of earth orbit, K is the product of the universal gravitational constant and the earth's mass.

UNCLASSIFIED

If a particle is released in such a force field at positions r_0 , θ_0 , and with velocities V_{r_0} and V_{θ_0} in the radial and polar angle directions it proceeds to orbit the center of force indefinitely with orbital characteristics:

Angular momentum (A2)

$$l_0 = r_0 V_{\theta_0} = \text{constant}$$

Apsidal radius (A3)

$$r_a = l_0^2 / K$$

Eccentricity (A4)

$$\alpha = \sqrt{r_a^2 V_{r_0}^2 + (r_0 - r_a)^2 V_{\theta_0}^2} / l_0$$

Phase angle relative to apogee (A5)

$$\cos(\theta_0 - \theta_a) = (1 - r_a / r_0) / \alpha$$

$$\sin(\theta_0 - \theta_a) = -(r_a V_{r_0}) / (\alpha l_0) \quad (A6)$$

The orbit then is described by (A7)

$$r = r_a / [1 - \alpha \cos(\theta - \theta_a)]$$

$$V_r = - [\alpha l_0 \sin(\theta - \theta_a)] / r_a \quad (A8)$$

$$V_\theta = l_0 / r \quad (A9)$$

It seems impossible to precisely specify the long term history of a particle ejected from a satellite, since the particle and satellite are separately subjected to uncertain solar wind pressure, weak radiation pressure, possible gravitational resonance/antiresonance with the moon and sun, higher harmonics of the earth's gravitational field, etc. In addition the satellite occasionally releases reaction mass which must modify the orbit to some extent, one part in 10^7 being of interest here. Therefore, we break this class of object into two subclasses, those which are observed on their first orbit, where we have confidence in our calculations, and those which are observed on some later orbit. This second class of object must be treated statistically.

UNCLASSIFIED

A.1.1 First Subclass - Particle Observed on First Pass

The problem is to eject an object from the VELA satellite by any means whatever (micrometeorite collision, thermo-mechanical stress, etc.) in such a way that Newton's orbital dynamics will cause the object to appear to swing around in front of the earth directed spin axis of the vehicle at appropriate velocity and distance.

In-Plane Perturbation

For the sake of simplicity, consider the main satellite (6911) to be in a circular orbit. The conclusion will not change for the small actual eccentricity of the orbit.

From the circular orbital point $r_1, \theta_1, V_{r_1} = 0, V_{\theta_1} = \sqrt{K/r_1}$ eject the object with very small relative velocity components δV_θ in the radial direction and δV_r in the polar direction.

To lowest order, the object has orbital parameters, obtainable by expansion of the above equations,

$$l = l_1 + r_1 \delta V_\theta = r_1 V_{\theta_1} (1 + \delta V_\theta / V_{\theta_1}) \quad (A10)$$

$$r_a = r_1 (1 + 2\delta V_\theta / V_{\theta_1}) \quad (A11)$$

$$\alpha = \sqrt{(\delta V_r)^2 + (2\delta V_\theta)^2} / V_{\theta_1} \quad (A12)$$

$$\sin(\theta_1 - \theta_a) = -\delta V_r / (\alpha V_{\theta_1}), \quad \cos(\theta_1 - \theta_a) = -2\delta V_\theta / (\alpha V_{\theta_1}) \quad (A13)$$

and orbit described by

UNCLASSIFIED

$$r = r_1 [1 + 2\delta V_\theta / V_\theta + \alpha \cos(\theta - \theta_a)] \quad (A14)$$

$$V_r = -\alpha V_{\theta_1} \sin(\theta - \theta_a) \quad (A15)$$

$$V_\theta = V_{\theta_1} [1 - \delta V_\theta / V_\theta - \alpha \cos(\theta - \theta_a)] \quad (A16)$$

A subsidiary quantity of particular interest is the angular velocity

$$\omega = V_\theta / r = \frac{V_{\theta_1}}{r_1} [1 - 3\delta V_\theta / V_\theta - 2\alpha \cos(\theta - \theta_a)] \quad (A17)$$

The first pass of the object occurs when both object and VELA have the same orbital polar angle at some time after release but before an orbital period has elapsed. It is considerably easier to calculate time as a function of angle from these equations rather than angle versus time. For the unperturbed orbit, the time is given by

$$t_u = \int d\theta / \omega_u = \int \frac{d\theta}{V_{\theta_1} / r_1} = (r_1 / V_{\theta_1}) \Delta\theta \quad (A18)$$

where $\Delta\theta \equiv \theta - \theta_1$

For the perturbed orbit,

$$\begin{aligned} t_p &= \int \frac{d\theta}{\omega_p} = \frac{r_1}{V_{\theta_1}} \int [1 + 3\delta V_\theta / V_\theta + 2\alpha \cos(\theta - \theta_a)] d\theta \quad (A19) \\ &= (r_1 / V_{\theta_1}) [\Delta\theta + 3(\delta V_\theta / V_{\theta_1}) \Delta\theta + 2\alpha \sin(\theta - \theta_a) + 2(\delta V_r / V_{\theta_1})] \end{aligned}$$

At the first pass, both the times are equal, so

$$3(\delta V_\theta / V_{\theta_1}) \Delta\theta + 2\alpha \sin(\theta - \theta_a) + 2(\delta V_r / V_{\theta_1}) = 0 \quad (A20)$$

UNCLASSIFIED

Writing out the expression for α , cancelling the V_{θ_1} in the denominator and dividing by $3\delta V_{\theta}$ leads to:

$$\Delta\theta + \frac{2}{3} \left[\frac{|\delta V_{\theta}|}{\delta V_{\theta}} \sqrt{4 + (\delta V_r / \delta V_{\theta})^2} \sin(\Delta\theta + \psi) + \delta V_r / \delta V_{\theta} \right] = 0 \quad (A21)$$

where $\psi \equiv \theta_1 - \theta_a$.

There are two possibilities for positive δV_{θ} . First, if δV_r is positive the pass occurs with object outside the VELA orbit where it can't be observed. Second, if δV_r is negative no solution exists for the first period, the object starts ahead and continues ahead of the VELA until the object crosses above the VELA orbit. Thus, the only potentially interesting cases are those with negative δV_{θ} ; consequently the factor $|\delta V_{\theta}| / \delta V_{\theta} = -1$.

Using A13 to find $\psi(\delta V_r / \delta V_{\theta})$ allows a numerical solution of A21 for $\Delta\theta$. Then substitution into A14 allows evaluation of the crucial ratio of the distance of passage to the initial polar velocity perturbation. Figure A1 shows a plot of ψ , $\Delta\theta$, and the ratio $(\delta r/r) / (\delta V_{\theta} / V_{\theta})$ for a range of radial-to-polar perturbation velocity ratios which exceeds the factor of about ten allowed by restriction 9 of Section 3.3.2.3. Equations A15 and A16 show that velocities observed at first passage are of the same order of magnitude as initial perturbed values.

The conclusion of importance from Figure A1 is that the distance of passage as a fraction of the orbital distance is comparable to the velocity perturbation as a fraction of orbital velocity. But the required transverse velocity is of order 10^{-2} or 10^{-3} of the orbital velocity while the required distance of passage is of order 10^{-7} of the orbital distance. It is clearly impossible for an in-plane perturbation to give the reflecting particle both the required velocity and the required separation from the satellite.

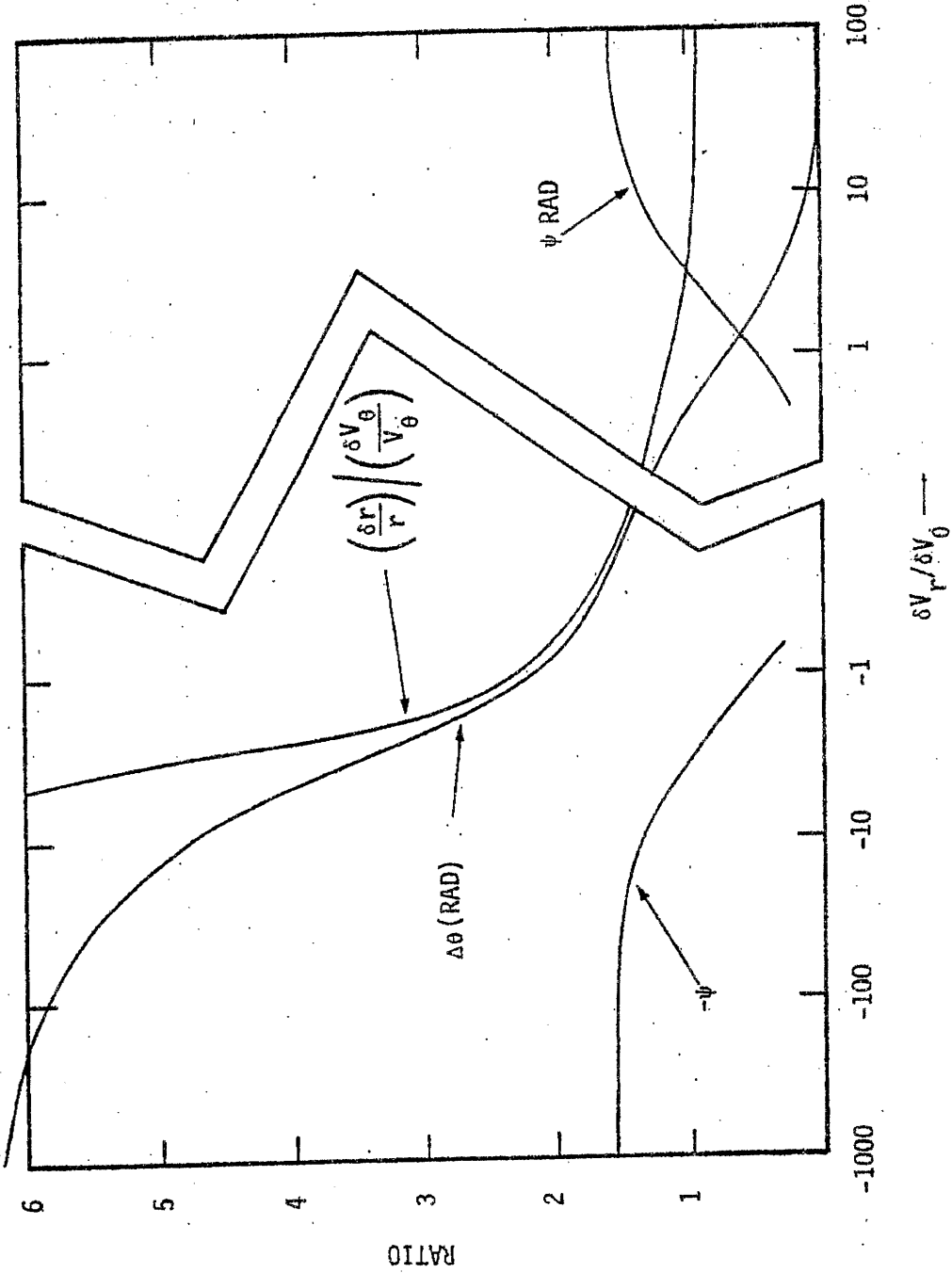


Figure A1. Solution to the "first passage" perturbation equations

UNCLASSIFIED

Out-of-Plane Perturbation

A perturbation in orbital velocity perpendicular to the orbital plane has no effect on the angular momentum or the apsidal radius, as is apparent from Equations A10 and A11. The only first order effect of such a perturbation is to tilt the orbital plane about the line joining the center of force to the satellite. The perturbed orbit then intersects the original twice per orbit, with only second order changes in timing.

On the surface this possibility sounds rather attractive, but more careful analysis shows it to be impalatable. In order to allow the intercept to occur within 10^{-7} of the orbital distance and within 10^{-2} of the orbital velocity, the angle of incremental velocity must be accurately perpendicular to the orbital plane within one part in 10^5 . If the direction of ejection is random as might be the case for meteorite impact, or indeed most mechanisms one could think of, then the probability of finding the right direction is

$$P \sim \left(\frac{\delta V}{V}\right)_\theta \left(\frac{\delta V}{V}\right)_r / 2\pi \sim 10^{-11} \quad (\text{A22})$$

per ejected particle.

If the particle is to have a radius as large as 0.1 mm, which is well below the limit found earlier for 10 m distance (i.e., 10^{-7} of orbital distance), then the volume of satellite ejected before a bit goes in the right direction is expected to be

$$V = \frac{4}{3} \pi r^3 / P \sim 4 \times 10^5 \text{ cm}^3 \quad (\text{A23})$$

which is somewhat larger than the volume of solid material in satellite 6911.

UNCLASSIFIED

Neither an in-plane nor out-of-plane perturbation seems capable of producing a first pass observation.

A.1.2 Second Subclass - Particle Observed on Later Pass

To obtain an estimate of the rate of occurrence of close approaches after the first orbit of an object ejected from a VELA satellite the following assumptions are made:

- (i) orbital perturbations on the VELA and the object are such as to modify the rate of rotation of an orbit in its plane without alteration of the semi-major axis or orbital eccentricity.
- (ii) to calculate mean rates we can regard phase of satellite versus object and apsidal precession as random.

These assumptions are quite optimistic in that alterations of semi-major axis and eccentricity as well as rotation of the orbital plane about an axis perpendicular to the ecliptic (rather than to itself) are ignored.

If the perturbation occurs in a random manner (rather than a peculiarly fortunate one) then, by expanding A14 near the orbital crossing and setting the sine to its upper limit of 1.0 ,

$$\frac{\Delta r}{r} \sim \alpha \Delta \theta \quad (A24)$$

In other words, the portion of the orbit which lies within $|\Delta r/r| \sim 10^{-7}$ is.

$$\frac{\Delta \theta}{2\pi} \sim \frac{10^{-7}}{\alpha} \sim 10^{-5} \quad (A25)$$

since $\delta V/V \sim 10^{-2}$ yields $\alpha \sim 10^{-2}$.

UNCLASSIFIED

This means that (a) the probability that VELA is on that portion of its orbit which intersects is $P_V \sim 10^{-5}$ and (b) given that VELA is on that portion of the orbit, the probability that the object also is there is $P_\theta \sim 10^{-5}$. Thus the combined probability is at best

$$P_c \lesssim 10^{-10} \quad (A26)$$

VELA's period is about 4 days. The number of orbits in a decade then is less than $N_o = 10^3$, and the probability that a satellite will have passed close enough to an object to observe it is less than

$$P_V = P_c N_o = 10^{-7} \text{ per object per VELA} \quad (A27)$$

Spherical objects at 10 m distance must have radii of order 1 cm, which implies a mass of order 10 gm. To be conservative, take the radius to be 1 mm, so the mass is, $m \sim 10^{-2}$ g. Then the expected mass of objects per VELA ejected prior to a close passage (not a bomb-like observation, not even an observation — just a close passage) is

$$M = m/P_V \sim 10^5 \text{ g} = 100 \text{ kg} \quad (A28)$$

This implies that all or at least a large fraction of the exposed area (mostly solar cells) on the VELA must be eroded before an optimist can expect a close passage.

One can improve the fraction of an orbit available for passage by about a factor of 10^2 by assuming the object to be ejected almost purely along the orbit at perigee or apogee, the peculiarly fortunate perturbation referred to earlier, but P_V is not improved because now the probability of being sufficiently close to perigee or apogee and of accurately aiming the particle must be included and these considerations more than eliminate all the gain.

UNCLASSIFIED

A.2 Electrostatic Orbit About the Spacecraft

In sunlit orbit beyond the magnetopause satellites are observed to acquire potentials as high as a few hundred volts.²⁵ This fact encourages the speculation that perhaps a particle originating on the satellite could be swung in front of the spin axis by electrostatic forces.

Let r_p be the radius of the particle, r_s be the radius of the satellite, V_p the potential of the particle and V_s the potential of the satellite (in esu, $V = \text{volts}/300$).

The charges on the two objects are, at best

$$Q_p = V_p r_p \quad (A29)$$

$$Q_s = V_s r_s \quad (A30)$$

and the force between them is

$$F = \frac{V_p V_s r_p r_s}{R^2} \quad (A31)$$

if R is the distance between their centers.

Assuming the potentials to somehow have opposite signs so that F is attractive, then the particle may swing in front of the satellite if

$$\frac{mv^2}{R} \sim F = \frac{V_p V_s r_p r_s}{R^2} \quad (A32)$$

where m is the mass of the particle

$$m = \frac{4}{3} \pi \rho r_p^3, \quad (A33)$$

UNCLASSIFIED

and v is the velocity across the field of view.

Restrictions necessary to produce the observed signal include

$$v \approx \alpha (R - r_s) \quad (A34)$$

where $\alpha = 1 \text{ sec}^{-1}$

and

$$r_p \approx \beta (R - r_s) \quad (A35)$$

where $\beta = 10^{-3}$.

Solving for ρ we find

$$\rho = \frac{V_p V_s r_s}{\frac{4}{3} \pi \alpha^2 \beta^2 R (R - r_s)^4} \quad (A36)$$

Taking V_p and V_s at the large values of 1 esu, r_s at the large value of 10^2 cm, and $(R - r_s)$ at the minimum value of 150 cm we find

$$\rho \sim 2 \times 10^{-4} \text{ g/cm}^3 \quad (A37)$$

This appears to be an unacceptable density for a physical object. If one wishes to consider a snowflake-like object of this extremely low density then the albedo should be down, thus β larger and ρ even less. Further, it is doubtful that an object of such highly structured shape could hold the electric charge corresponding to several hundred volts. This mechanism then does not appear credible.

UNCLASSIFIED

REFERENCES

1. J.J. McGee, letter to D.S. Sappenfield dated 7 November 1979. (S)
2. R.E. Wiley and D.H. Good, "Alert 511 Optical Data Analysis (U)" AFTAC-TR-73-13, August 1973. (S)
3. J. van Workham, J.D. Marshall, private communications, November 1979. (S)
4. R.E. Wiley, L.W. Seiler, Jr., and J.J. Lange, "Optical Scaling Laws (U)" AFTAC-TR-80-3, January 1980. (SFRD-██████████) AF b(2)
5. D.S. Sappenfield and T.H. McCartor, "The Surface-Burst Correction Factor for Bhangmeter Scaling Laws (U)" AFTAC-TR-79-12, March 1979. (SRD)
6. D.S. Sappenfield and T.H. McCartor, "Yield and Height of Burst Determination for High Altitude Nuclear Explosions (U)" AFTAC-TR-79-71, August 1979. (SRD)
7. D.S. Sappenfield, "Emplacement Effects on Optical Signals (U)" AFTAC-TR-78-14, February 1978. (S-██████████) AF b(2)
8. D.S. Sappenfield and T.H. McCartor, "Optical Data Evaluation Technology - Second Annual Report (U)" AFTAC-TR-79-13, March 1979. (S-██████████) AF b(2)
9. D.S. Sappenfield and W.A. Schlueter, "Early-Time Optical Studies - III (U)" Mission Research Corporation, MRC-R-178, May 1975. (SRD)
10. J. Zinn, J. Comp. Phys., 13, 569. (1973). (U)
11. D.S. Sappenfield, "Early-Time Optical Studies IV (U)" Mission Research Corporation, MRC-R-283, September 1976. (S)
12. R. Whitaker and H. Horak, "Calculations..... (U)" Paper presented at the Satellite Working Group Meeting, PAFB, 18-20 March 1980. (S)

UNCLASSIFIED

13. R. Hillendahl, "Interpretation....(U)" Paper presented at the Satellite Working Group Meeting, PAFB, 18-20 March 1980. (S)
14. P.B. Wells, et al., "Nuclear Weapons Thermal Radiation Phenomena (U)" DNA 2500H-2, July 1974. (SRD)
15. W.L. Derksen and F.C. DeBold, "Measured Spectral Powers for Ten Low Altitude Nuclear Bursts (U)" DASA-1663-4, January 1972. (SFRD)
16. G. Mauth, Informal presentation at the Satellite Working Group Meeting, PAFB, 18-20 March 1980. (S)
17. J.D. Marshall, "Statistical Analysis (U)" Paper presented at the Satellite Working Group Meeting, PAFB, 18-20 March 1980. (S)
18. S. Chavin, T.H. McCartor and D.S. Sappenfield, "Yield and Depth of Burial Determination for Shallow-Buried Nuclear Bursts (U)" AFTAC-TR-78-49, July 1978. (S-██████████) AF b(2)
19. L.W. Seiler, Jr., J.A. Van Workham and N.P. Philliber, "Satellite Data Summary ██████████ (U)" AFTAC-TR-79-9, March 1979. (S) AF b(2)
20. Turman, B.N., "Detection of Lightning Superbolts," J. Geophys. Res., 82; 2566 (1977). (U)
21. Turman, B.N., "Lightning Detection From Space," Am. Sci., 67, 321 (1979). (U)
22. Edgar, B.C., "Global Lightning Distribution at Dawn and Dusk for August-December 1977 as Observed by the DMSP Lightning Detector," The Aerospace Corporation, SSL-78(3639-02)-1, August 1978. (U)
23. Uman, M.A., Lightning, McGraw-Hill Book Company, New York, 1979. (U)
24. Marshall, J.D., private communication, December 1979. (U)
25. DeForest, S.E., "Spacecraft Charging at Synchronous Orbit," J. Geophys. Res., 77, 651 (1972). (U)